A Survey of 5G Channel Measurements and Models

Cheng-Xiang Wang, *Fellow, IEEE,* Ji Bian, Jian Sun, *Member, IEEE,* Wensheng Zhang, *Member, IEEE*, and Minggao Zhang

Abstract—The fifth generation (5G) mobile communication systems will be in use around 2020. The aim of 5G systems is to provide anywhere and anytime connectivity for anyone and anything. Several new technologies are being researched for 5G systems, such as massive multiple-input multiple-output (MIMO) communications, vehicle-to-vehicle (V2V) communications, high-speed train (HST) communications, and millimeter wave (mmWave) communications. Each of these technologies introduces new propagation properties and sets specific requirements on 5G channel modeling. Considering the fact that channel models are indispensable for system design and performance evaluation, accurate and efficient channel models covering various 5G technologies and scenarios are urgently needed. This paper first summarizes the requirements of the 5G channel modeling, and then provides an extensive review of the recent channel measurements and models. Finally, future research directions for channel measurements and modeling are provided.

Index Terms—5G communication systems, channel modeling requirements, channel measurements, channel models, statistical properties.

I. INTRODUCTION

The fifth generation (5G) systems will enable people to access and share information in a wide range of scenarios with extremely low latency and very high data rate [1]. It should achieve 1000 times the system capacity, 100 times the data rate, 3–5 times the spectral efficiency, and 10–100 times the energy efficiency with respect to the current fourth generation (4G) systems [2], [3]. One of the most promising technologies in 5G systems is millimeter wave (mmWave) communication [4]. Benefiting from the very large bandwidth, mmWave communication is able to provide a data rate of several gigabits per second with ease. Higher frequency propagation introduces severe path loss. However, if we consider small cells with radii of 100–200 m, the mmWave communication can achieve satisfactory performance [5]. Another approach to overcome high path loss is beamforming, which can be achieved through combining with massive multiple-input multiple-output (MIMO) technologies. A high-gain steerable antenna array is able to transmit or receive signals in specific directions, getting

C.-X. Wang is with the State Key Laboratory of Mobile Communications, Southeast University, Nanjing, 210096, China (e-mail: chxwang@seu.eu.cn).

J. Bian, J. Sun (corresponding author), W. Zhang, and M. Zhang are with Shandong Provincial Key Lab of Wireless Communication Technologies, School of Information Science and Engineering, Shandong University, Qingdao, Shandong, 266237, China. (e-mail: bianjimai@163.com; sunjian@sdu.edu.cn; zhangwsh@sdu.edu.cn; zmg225@163.com).

around obstructions, and compensating for severe path loss [6]. Besides, massive MIMO can greatly increase the capacity and reliability of the system with respect to the conventional MIMO [7], [8].

The 5G systems are assumed to provide seamless coverage and high-quality connectivity between various devices and behave well under diverse network topologies, such as multi-hop networks, moving networks, device-to-device/vehicle-to-vehicle (D2D/V2V) communications, etc. Furthermore, 5G systems should be adapted to a wide range of scenarios, such as indoor, urban, suburban, rural area, etc. All the above-mentioned technologies set new requirements for 5G channel modeling, which are summarized as follows:

1) Wide Frequency Range: A new 5G channel model should support a wide frequency range, e.g., 350 MHz to 100 GHz. The model at higher frequency bands, e.g., above 6 GHz, should maintain compatibility with the model at lower frequency bands, e.g., below 6 GHz.

2) Broad Bandwidths: A new 5G channel model should have the ability to support large channel bandwidths, e.g., 500 MHz to 4 GHz.

3) Wide Range of Scenarios: A new 5G channel model should be able to support a wide range of scenarios such as indoor, urban, suburban, rural area, high-speed train (HST) scenarios, etc.

4) Double-Directional Three-Dimensional (3D) Modeling: A new 5G channel model should provide full 3D modeling, including accurate 3D antenna modeling and 3D propagation modeling.

5) Smooth Time Evolution: A new 5G channel model has to evolve smoothly over time, involving parameters drifting and cluster fading in and fading out, which are important to support mobility and beam tracking for 5G communications [9].

6) Spatial Consistency: Spatial consistency means two closely located transmitters or receivers should have similar channel characteristics. Channel states including large-scale parameters (LSPs), small-scale parameters (SSPs), line-of-sight/non line-of-sight (LoS/NLoS) condition, and indoor/outdoor state should vary in a continuous and realistic manner as a function of position [10].

7) Frequency Dependency and Frequency Consistency: The parameters and statistics of a new 5G channel model should vary smoothly with the frequency. Channel parameters and statistics at adjacent frequencies should have strong correlations.

8) Massive MIMO: A new 5G channel model must support massive MIMO, i.e., spherical wavefront and array non-stationarity have to be properly modeled [10].

— *Spherical wavefront:* In massive MIMO systems, the distance between the transceiver and cluster could be less than

the Rayleigh distance. Therefore, spherical wavefront instead of plane wavefront must be considered.

— *Array non-stationarity:* Array non-stationarity refers to the fact that clusters may appear or disappear from the viewpoint of one antenna element to the next one, which means different antenna elements could see different cluster sets. It also means parameters, such as power and delay drift, over different antenna elements.

9) Direct D2D/V2V: In D2D/V2V scenarios, both the transmitter and receiver are equipped with lower antennas and may interact with a large number of scatterers. D2D/V2V channel models have to take into account the mobility of both ends, which significantly increases the modeling complexity. The relative speed between the two ends and fast-changing environments introduce extra Doppler frequency shift and result in serious non-stationary channels [11], [12]. All of these make the D2D/V2V channels differ greatly from conventional cellular channels.

10) High Mobility: A new 5G channel model should support high mobility scenarios, such as HST scenario with the speed of the train even over 500 km/h. The model should be able to capture certain characteristics of high mobility channels, such as large Doppler frequency and non-stationarity. Furthermore, the channel model has to work reliably in various HST scenarios, including open space, viaduct, cutting, hilly terrain, tunnel, station scenarios, etc.

Although there are a large number of papers on 5G channel measurements and models, the number of tutorial/survey papers on 5G channel measurements and models is very limited. Besides, most of them concentrated on certain topics, e.g., [13] and [14] for massive MIMO communication scenarios, [15]–[17] for V2V communication scenarios, [18] and [19] for HST communication scenarios, [5] and [20] for mmWave communication scenarios. All the above-mentioned papers cannot completely clarify the 5G channel modeling requirements. To the best of the authors' knowledge, a survey paper for 5G channel measurements and models covering various 5G technologies/scenarios and presenting the latest channel models of different standardization organizations is still missing. This paper aims to fill this gap. The major **contributions** of this paper are summarized as follows:

1) The requirements for 5G channel modeling are highlighted. The most important channel measurements are reviewed in terms of different scenarios (applications and frequency bands). New propagation characteristics are introduced and their underlying propagation mechanisms are discussed.

2) The scenario-specific 5G channel models are presented. For each scenario, the state-of-the-art modeling approaches are introduced and compared in a comprehensive manner.

3) General 5G channel models covering more scenarios and proposed by different organizations are presented. The pros and cons of each general models are discussed. A comprehensive comparison of those models is proposed.

4) Future research directions for 5G and beyond 5G (B5G) channel measurements and modeling are outlined.
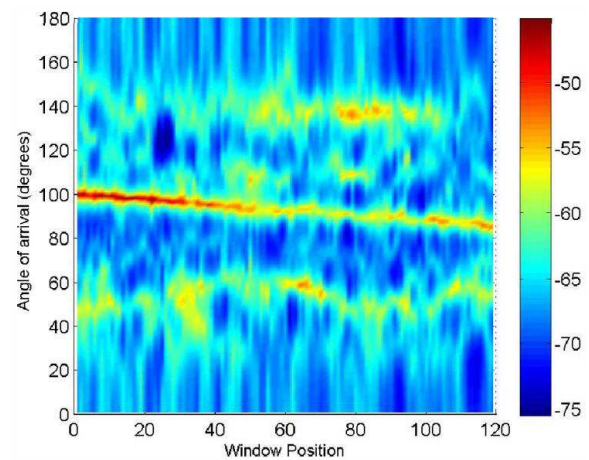

Fig. 1. APSs over the array in the LoS case [21].

The rest of this paper is organized as follows. In Section II, an overview of 5G channel measurements and propagation properties is presented. Existing 5G channel models for various scenarios are provided in Section III. General 5G channel models covering more scenarios are introduced in Section IV. Future research directions for 5G and B5G channel measurements and models are outlined in Section V. Finally, conclusions are drawn in Section VI.

II. 5G CHANNEL MEASUREMENTS

In this section, we will briefly review several representative channel measurements in the light of different 5G communication technologies. New propagation properties caused by 5G communication technologies in different propagation environments were reported in the following measurement campaigns and should be considered carefully in 5G channel modeling.

A. Massive MIMO Channel Measurements

In massive MIMO communication systems, hundreds or even thousands of antennas are equipped at one end or both ends. A large number of antennas make the massive MIMO channels exhibit non-stationary properties across the array, which are distinctly different from the case of conventional MIMO channels [13]. In [21], channel measurements were conducted at 2.6 GHz with a bandwidth of 50 MHz and a virtual 128-element linear array was used at the base station (BS). Significant variations of the channel gain, K-factor, and angular power spectrum (APS) over the linear array were observed. As shown in Fig. 1, the angle of arrival (AoA) of the LoS path gradually shifts from $100°$ to $80°$ across the 7.3 m linear array, which indicates that the plane wave assumption or far-field assumption is not valid in massive MIMO systems. Furthermore, measurement results show that the clusters in the propagation environment can appear and disappear along the array. Some clusters are visible over the whole array, while other clusters can only be seen by part of the array. Besides the linear array, other forms of large antenna array were also reported in massive MIMO channel measurements. In [22],

measurements were conducted at 15 GHz with a bandwidth of 4 GHz. A virtual 40×40 (1600 elements) planar antenna array was used and divided into several 7×7 sub-arrays in order to investigate the non-stationary behaviors of massive MIMO channels over the array. Measurements show that the K-factor, delay spread, azimuth angular spread of arrival (AASA), and elevation angular spread of arrival (EASA) vary in blocks with clear borders over the array plane. The birth and death behavior of clusters across the array aperture can also be observed. Recently, massive MIMO channel measurements in an indoor office environment at 11, 16, 28, and 38 GHz bands were conducted [23]. The measurements were carried out using a vector network analyzer (VNA) and a large virtual uniform rectangular array (URA). The element spacing was set to half-wavelength and the total numbers of array elements for the four mmWave bands were 51×51, 76×76, 91×91, and 121×121. The multipath component (MPC) parameters were extracted using the space-alternating generalized expectation-maximization (SAGE) algorithm. Massive MIMO propagation properties including spherical wavefront, cluster appearance and disappearance, and parameters drifting over the array were verified and analyzed.

Apart from the channel non-stationarity over the antenna array, some measurements investigated the impacts of array structures on the massive MIMO system performance. Measurements in [24] and [25] were performed in a campus at 2.6 GHz with a bandwidth of 50 MHz. A virtual uniform linear array (ULA) and a uniform cylindrical array (UCA) were used in those measurements. Both the ULA and UCA contain 128 antenna elements with an element spacing of a half-wavelength. The antennas of the ULA are spread along a line of 7.3 m. The antennas of the UCA are distributed in a cylinder with both diameter and height of about 30 cm. The authors found that channels using ULA exhibit more significant array non-stationarity and better user decorrelation, and can achieve higher sum-rate capacities compared to the channels using UCA. Besides, the massive MIMO channels in both cases have better spatial separation, user channel orthogonality, and channel stability than conventional MIMO channels. Furthermore, measurement results show that channels in NLoS conditions with rich scattering exhibit better spatial separation and user channel orthogonality compared to channels in LoS cases. In [26], measurements were performed in an indoor canteen environment at 5.8 GHz with 100 MHz bandwidth. A total of 64 antennas were used and rearranged into 3 different array shapes, i.e., a square compact two-dimensional (2D) rectangular array of 25 cm×28 cm, a large aperture linear array of 2 m long, and a very large aperture linear array of 6 m long. Measurement results illustrate that the array with the largest aperture (dimension) provides the best user orthogonality and achieves the best performance close to that of the independent and identically distributed (i.i.d.) channel. Significant power variations across arrays were observed and the linear array with the largest aperture shows the largest power variations. Note that for the compact 2D array, power variations of more than 10 dB were even observed. Compared to the UCA and rectangular array, the larger aperture size of ULA brings some advantages such as better spatial separation and batter user

orthogonality. However, the ULA only has angular resolution in one dimension. The UCA and rectangular array can resolve waves in two dimensions. Besides, from a practical point of view, antenna arrays with smaller sizes are easier to deploy.

B. V2V Channel Measurements

A series of V2V channel measurements have been performed in various scenarios, such as open highway [27], suburban [28], campus [29], crossroad [30], etc. Measurement results show that fading amplitudes of V2V channels are best fitted with the Nakagami distribution. When vehicles move within a short distance, fading amplitudes tend to be Rician distributed due to the strong LoS path. When the distance between the two vehicles increases, the LoS path becomes weaker and fading amplitudes tend to be Rayleigh distributed. However, the measurements in [31] performed in highways and cities indicated that fading amplitudes of V2V channels are better fitted with the Weibull distribution than the Nakagami distribution. Measurements in [32] found that fading amplitudes are best fitted by both the Nakagami and Weibull distributions. Besides, delay spread, as one of the key parameters, describes the spread of the delay around the mean delay and indicates the multipath richness of the channel. Depending on different propagation scenarios and traffic volumes, the root-mean-square (RMS) delay spread of V2V channels ranges from about several tens of nanoseconds to several hundreds of nanoseconds [11], [33]. References [27] and [34] indicate that the RMS delay spread can be fitted by the log-normal distribution. Perhaps the biggest difference between V2V channels and conventional cellular channels is the Doppler spread. V2V channels often have large Doppler spread due to the fast-changing environments and high relative speed between the transmitter and receiver. Measurements in [16] and [33] show that the mean Doppler spreads of most V2V channels are in the order of 100–300 Hz when vehicles move at speeds between 50–80 km/h and measurements conducted with a center frequency of 5.9 GHz. With the same center frequency and vehicle speeds, large Doppler shifts up to 1100 Hz or higher resulting from reflections off the approaching vehicles were reported in [11]. V2V channel measurements in [35], which were conducted in a traffic congestion situation and under NLoS conditions, found that traffic signs, trucks, and bridges instead of other cars contribute to the most of the multipath propagation.

Most V2V channels can be considered as non-stationary due to the fast changes of propagation environments. V2V channel measurements in [33] were performed in urban and suburban scenarios and found that both the RMS delay spread and RMS Doppler spread are time-varying and frequency-varying. In [35], a non-stationary V2V channel was characterized by its time-varying power delay profile (PDP) and time-varying Doppler power spectrum density (PSD). Authors in [31] indicated that a MPC may exist in a short duration, i.e., appears, remains for a certain time span, and then disappears, which can be generated by a reflector/scatterer, such as a large moving truck. The random on/off behavior of MPCs can be modeled by a "persistence process". Through evaluations

of a wide range of V2V channel measurements, authors in [36] proved that the fading processes of V2V channels are neither wide-sense stationary (WSS) nor uncorrelated scattering (US). Authors in [37] investigated the non-stationarity of V2V channels using a metric called correlation matrix distance (CMD), which is defined as the distance between channel correlation matrices at different times. In [32], a similar method was used in order to investigate the non-stationarity of V2V channels in campus, highway, urban, and suburban scenarios. Authors found that different taps of V2V channels have different stationary distances (maximum distance over which the CMD exceeds a certain threshold) due to the appearance and disappearance of MPCs. The median stationarity distance was estimated in the range of 15–40 m when the cars move in the same direction with a speed of 5–15 km/h.

C. HST Channel Measurements

In order to investigate the HST channel characteristics, a series of HST channel measurements have been conducted, including measurements at 2 GHz with speeds of 220–270 km/h between Beijing and Shanghai in China [38], measurements at 930 MHz with speeds of 200–350 km/h between Zhengzhou and Xian in China [39]–[46], measurements at 2.4 GHz with a speed of 295 km/h between Guangzhou and Shenzhen in China [47], measurements at 5.25 GHz with three different speeds, i.e., 20, 100, and 240 km/h between Siegburg and Frankfurt in Germany [48], measurements at 2.35 GHz with a speed of 240 km/h between Beijing and Tianjin in China [49], and measurements at 2.35 GHz with a speed 200 km/h between Zhengzhou and Xian in China [50].

Most HST channel measurements concentrated on large-scale fading [38]–[41], [47]. Measurement results confirm that the path loss of HST channels fits the classical log-distance path loss model [51] and the shadowing fits the log-normal distribution. The measurement results also show that the large-scale fading is largely affected by the detailed structures of propagation environments. Measurements in [40] show that the path loss of HST channels in viaduct scenarios is influenced by the viaduct height and the BS antennas height, i.e., higher viaducts result in larger path loss exponents (PLEs), whereas higher BS antennas lead to smaller PLEs. Measurements in [41] show that a larger slope of the cutting wall results in a larger path loss for both low and deep cutting scenarios. However, the shadowing is significantly influenced by the cutting depth, i.e., a deeper cutting leads to larger shadow. Measurements in [42] indicated that in cutting scenarios, both the PLE and shadowing standard deviation of the log-normal distribution are larger than those in viaduct scenarios. For the small-scale fading, the dynamic fading range, which is defined as the difference between the minimum and the maximum of the signal amplitude within an observation window, in cutting scenarios is also larger than the value in viaduct scenarios. The bridges built over the cuttings cause an extra loss of about 5 dB. Authors in [47] indicate that the path loss of HST channels in hilly scenarios fits a two-slope curve.

Authors in [43] and [44] characterized the small-scale fading of HST channels by fade depth, which is defined as the difference between the 50% and 1% of cumulative distribution of received signal powers in dB. They showed that the fade depth is around 15 dB for a viaduct scenario and around 17 dB for a cutting scenario. Most HST scenarios can be considered as typical LoS conditions. Authors in [43] illustrated that the fading envelopes fit the Ricean distribution. K-factor is an important parameter to characterize the fading envelopes of HST channels, which indicates the power ratio of the LoS component to all other scattering components. Authors in [41] and [39] showed that the K-factor of HST channels fits the log-normal distribution. The mean values of the K-factors have been reported in various HST scenarios, e.g., 6 dB for an open space scenario [48], 4.55 dB for a viaduct scenario [43], 1.52 dB for a cutting scenario [44], and 0.72 dB for a hilly terrain scenario [47].

HST channels are distinctly characterized by its non-stationarity due to the high speed of the train. Measurements in [49] show that the K-factor, multipath characteristics, and Doppler features vary dramatically with the location of the train. However, few measurements were conducted to capture the non-stationarity of HST channels. Authors in [45] and [46] measured the stationary interval of HST channels with local region stationarity (LRS) metric, which is defined as the time over which the correlations of consecutive averaged power delay profiles (APDPs) exceed a certain threshold. Based on the LRS metric, at 324 km/h the stationary interval of the HST channel was estimated as 9 ms. This is much shorter than the stationary interval of standardized channel models, such as spatial channel model (SCM), WINNER II, and IMT-Advanced channel models. The LRS quantifies the stationary interval in the power domain, whereas authors in [45] adopted the CMD [52] to analyze the non-stationarity of HST channels regarding the changes of the spatial structure of the MIMO channel. Authors in [50] quantified the non-stationarity of HST channels in a cutting scenario with another metric called non-stationary index, which is defined as the difference between the value and time average value of the autocorrelation of time-variant transfer function.

D. MmWave Channel Measurements

Most mmWave channel measurements concentrated on severe path loss, which is the biggest challenge for the application of mmWave communication. According to the free space propagation equation, the received power is proportional to the inverse square of the carrier frequency, revealing a large path loss of mmWave transmission. Measurements in [5], [20], and [53]–[57] were carried out at 28 GHz, 38 GHz, 60 GHz, and 73 GHz in New York. Measurement results show that the omnidirectional PLEs are in the range of 1.8–2.1 for the LoS case and 2.4–3.5 for the NLoS case, and increase slightly as the carrier frequency increases. The path loss at mmWave bands in the LoS case can be accurately described by the Friis equation. Apart from the path loss, atmospheric absorption and rain attenuation can also lead to a significant power loss at mmWave bands. Measurements in [58] show that attenuations caused by atmospheric absorption and heavy rain at 28 GHz over a distance of 200 m are about 0.012 dB and

1.4 dB, respectively. Considering the above-mentioned facts, most mmWave communications will be deployed in small cells with an inter-site distance of up to 200 m [5]. Short wavelength makes mmWave more sensitive to the objects such as foliage, human, and vehicle. It is indicated that swaying foliage can cause a 10 dB attenuation at 29.5 GHz, but only 2 dB attenuation at 5 GHz [59]. Measurements at 26 GHz and 39.5 GHz show that 1–3 walking person(s) can result in an attenuation of 12.53–33.98 dB [60].

The authors in [61] conducted 28 GHz channel measurements, which focused on reflection coefficients and penetration losses of different materials. Measurement results show that outdoor materials usually have higher reflection coefficients, e.g., 0.815 for concrete, whereas the reflection coefficients of indoor materials are relatively lower, e.g., 0.74 for clear glass. Meanwhile, the penetration loss of outdoor materials is generally high, e.g., 40.1 dB for tinted glass, and the penetration loss of indoor materials is relatively low, e.g., 3.9 dB for clear class. The high reflection coefficients and large penetration losses of outdoor materials make the mmWave hard to penetrate into the walls between indoor and outdoor. However, it helps to reduce inter-cell interference. More detailed reflection coefficients and penetration losses of different materials at mmWave bands were reported in [61]–[63].

The high frequency or short wavelength of mmWave results in weak diffractions which make the mmWave exhibit quasi-optical properties. In mmWave transmissions, most of the propagation power is contributed by the LoS and low-order reflected components [64]. Measurements in [65] were performed in an office at 60 GHz with a 800 MHz bandwidth and using directional antennas of 18 dB. It was shown that the powers of the LoS component, first-order reflection components, and second-order reflection components are about 30 dB, 15–20 dB, and 2–6 dB over noise level, respectively. Measurements in [66] were conducted at 81–86 GHz in street canyon and roof-to-street environments and found that the LoS component is at least 20 dB higher than the first MPC. As the frequency increases, according to the Rayleigh criterion [51], more surfaces will be identified as rough, leading to more diffuse scattering and less reflections at mmWave bands [67]. In mmWave communications, highly directional antennas are often used in order to cope with the large attenuation, resulting in smaller delay spreads. Various measurements performed at 28–73 GHz using different directional antennas find the delay spreads are typically less than 20 ns [68]–[71]. In the spatial domain, measurements in [5], [20], and [71]–[73] show that the number of scattering clusters in mmWave bands is much less than that in frequency bands of below 6 GHz. In [74], 60 GHz channel measurements were carried out in an indoor office environment. MPC parameters such as azimuth angle of departure (AAoD), elevation angle of departure (EAoD), azimuth angular spread, elevation angular spread, Rician factor, and ray arrival rate were obtained. Measurement results illustrate that the azimuth angular spread is much larger than the elevation angular spread. The AAoDs are significantly affected by the antenna position and the propagation environment. However, the EAoDs are more influenced by the antenna height difference.
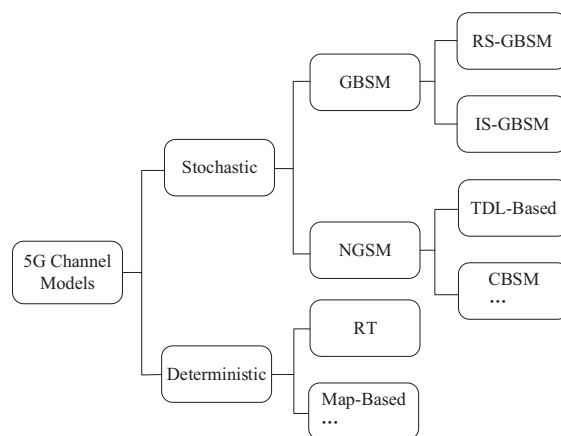

Fig. 2. Classification of 5G channel models.

E. Summary for 5G Channel Measurements

A comparison of 5G channel measurement campaigns is shown in Table I. It is worth noting that 5G systems will employ and combine different revolutionary technologies and work reliably in various environments. However, only few measurement campaigns considered employing multiple technologies together, e.g., mmWave massive MIMO channel measurements [23]. Similar measurement campaigns such as massive MIMO V2V channel measurement, mmWave HST channel measurement, etc., should be carried out in the future. Furthermore, few measurements were conducted under new scenarios, e.g., crossroad [30] and parking garage [63]. Future measurements should be carried out under more scenarios, such as airport, train station, shopping mall, gymnasium, etc.

III. SCENARIO-SPECIFIC 5G CHANNEL MODELS

According to the modeling approach, channel models can be classified into stochastic channel models and deterministic channel models. Stochastic channel models describe channel parameters using certain probability distributions. Generally speaking, stochastic channel models are mathematically tractable and can be adapted to various scenarios with relatively low accuracy (compared with deterministic channel models). Deterministic channel models predict the propagation waves in a more accurate manner by solving the Maxwells equations or approximated propagation equations. Deterministic channel models usually introduce high computational complexity and rely on precise information of the propagation environments. More detailed classification of 5G channel models and their definitions can be found in Fig. 2 and Table II, respectively. In this section, 5G channel models in the literature are reviewed and classified in terms of different communication technologies or scenarios. These technologies introduce distinctly different propagation characteristics compared to those of conventional channels and pose new challenges to the 5G channel modeling. We will briefly introduce these challenges and review the approaches to overcome them.

TABLE I
IMPORTANT 5G CHANNEL MEASUREMENTS.

Ref	Category	Scenario	Carrier Frequency	Antenna	Channel Statistics
[21]	massive MIMO	court yard	2.6 GHz	virtual LA	K-factor, APS, antenna correlation, user correlation
[22]	massive MIMO	top of building	15 GHz	virtual PA	K-factor, delay spread, angular spread, number of clusters
[23]	massive MIMO, mmWave	indoor office	11, 16, 28, 38 GHz	virtual RA	APDP, PAP, PEP, delay spread, angular spread, antenna correlation, capacity
[24], [25]	massive MIMO	campus	2.6 GHz	virtual LA, CA	user decorrelation, user orthogonality, singular value spread, capacity
[26]	massive MIMO	indoor canteen	5.8 GHz	RA, LA	path power, user orthogonality, eigenvalue, condition number
[27]	V2V	urban, open highway	5.12 GHz	SISO	FCF, delay spread, fading amplitude
[28]	V2V	suburban	5.9 GHz	SISO	path loss, Doppler spread, coherence time
[29]	V2V	campus, urban	5.8 GHz	SISO	path loss, shadowing, fading amplitude, delay spread
[30]	V2V	crossroad	5.3 GHz	semi-SA, ULA	fading amplitude, stationary interval, delay spread, angular spread
[31]	V2V	urban, highway	5.12 GHz	SISO	fading amplitude, FCF
[32]	V2V	campus, highway, urban, suburban	5.3 GHz	semi-SA	fading amplitude, inter-tap correlation, CMD
[38]	HST	viaduct	2 GHz	SISO	PLE, shadowing
[39]–[46]	HST	viaduct, cutting	930 MHz	SISO	fading amplitude, path loss, shadowing, fading depth, K-factor, LCR, AFD, stationary interval
[47]	HST	hilly terrain	2.4 GHz	SISO	path loss, shadowing, K-factor
[48]	HST	open space	5.25 GHz	SIMO, UCA	path loss, shadowing, K-factor, delay spread, angular spread, number of clusters
[49]	HST	viaduct	2.35 GHz	SISO	path loss, delay spread, K-factor
[50]	HST	cutting	2.35 GHz	SISO	channel gain, non-stationary index
[5], [20], [53]–[57], [69]–[72]	mmWave	urban, suburban	28, 38, 60, 73 GHz	RDA	path loss, shadowing, penetration loss, reflection coefficient, delay spread, angular spread
[58]	mmWave	urban	35, 103 GHz	SISO	rain attenuation
[59]	mmWave	urban	29.5 GHz	SISO	foliage attenuation
[60]	mmWave	indoor restaurant	26, 39.5 GHz	SISO	human body attenuation
[61]	mmWave	in and around building	28 GHz	SISO	reflection coefficient, penetration loss
[62]	mmWave	indoor office	57.5 GHz	SISO	reflection coefficient, penetration loss
[63]	mmWave	indoor, parking garage	28, 40 GHz	SISO	reflection coefficient, penetration loss, PLE
[65]	mmWave	indoor office	60 GHz	RDA	fading amplitude, K-factor, ray arrival rate, average number of rays
[66]	mmWave	street canyon, roof-to-street	83.5 GHz	SISO	fading amplitude
[68]	mmWave	urban	59 GHz	SISO	mean delay, delay spread, delay interval, delay window
[73]	mmWave	indoor, urban, O2I	15, 17, 28, 60, 86 GHz	RDA	path loss, shadowing, K-factor, fading depth, delay spread, angular spread, number of clusters, number of rays per cluster
[74]	mmWave	indoor office	60 GHz	virtual RA, RDA	K-factor, fading amplitude, delay spread, angular spread, PAP, PEP

LA: linear array; PA: planar array; RA: rectangular array; CA: cylindrical array; SA: spherical array; ULA: uniform linear array; UCA: uniform cylindrical array; RDA: rotated directional antenna; APS: angular power spectrum; APDP: averaged power delay profiles; PAP: power azimuth profile; PEP: power elevation profile; FCF: frequency correlation function; CMD: correlation matrix distance; LCR: level crossing rate; AFD: average fade duration; PLE: path loss exponent

A. Massive MIMO Channel Models

In massive MIMO channels, due to the large dimension of antenna array, the distance between the transmitter/receiver and the cluster may be shorter than the Rayleigh distance, which is defined as $2L^2/\lambda$, where L is the aperture size of the antenna array and λ is the wavelength [75]. Therefore, the far-field condition is not fulfilled. The spherical wavefront instead of plane wavefront should be considered. Besides, massive MIMO channels are strikingly characterized by their array non-stationarity. Specifically, different antennas can see different cluster sets. Path parameters such as power and delay can drift over different antennas. All the above-mentioned challenges should be addressed in massive MIMO channel modeling.

Most massive MIMO channel models in the literature are based on the mature geometry-based stochastic models (GBSMs) and extended with new features, e.g., spherical wavefront and array non-stationarity. Authors in [75]–[78] proposed massive MIMO channel models based on a twin-cluster model, an ellipse model, a multi-ring model, and a twin-multi-ring model, respectively. Appearance and disappearance of the clusters over the array were modeled by a Markov process or a birth-death process. The spherical wavefront was obtained by calculating the distances between every transceiver element and clusters. The parameter drifts over the array were calculated based on the geometry. A major improvement was reported in [79], where the authors proposed a 2D WINNER-like massive MIMO channel model. The cluster generation and

TABLE II
DEFINITIONS OF CHANNEL MODELING APPROACHES.

Modeling Approach	Definition
RS-GBSM	Scatterers are assumed to be stochastically distributed according to a particular underlying geometry with a regular shape.
IS-GBSM	Scatterers are assumed to be stochastically distributed without being located on a regular shape.
TDL-based	Defined as a summation of a series of complex gains with different time delays.
CBSM	Describe the spatial structure of a MIMO channel by modeling the correlation between antenna elements.
RT	Rays are determined and calculated according to the geometric optic (GO), geometric theory of diffraction (GTD), and uniform theory of diffraction (UTD) approximations of electromagnetic fields.
Map-based	Based on RT method using a simplified 3D map where propagation mechanisms such as diffraction and specular reflection can be turned on or off

Fig. 3. Extension of cluster visibility regions to the base station side [82].

recombination were simulated by a two-state Markov process. A spatial log-normal process was adopted to provide smooth power variations. The authors proposed a new approximation algorithm for calculating spherical wavefront, i.e., parabolic wavefront, which can model linear angular drifts of MPCs over large arrays and at the same time reduce computational complexity. The relationships among plane wavefront, spherical wavefront, and parabolic wavefront can be expressed as [79]

$$R_{c,p} = \underbrace{\sqrt{R_c^2 + x_p^2 - 2R_c x_p \cos(\alpha)}}_{\text{spherical wavefront}}$$

$$\approx \underbrace{\overbrace{R_c - x_p \cos(\alpha)}^{\text{plane wavefront}} + \frac{x_p^2}{2R_c} \sin^2(\alpha)}_{\text{parabolic wavefront}} \quad (1)$$

where $R_{c,p}$ and R_c are the distances from the cth cluster to the pth antenna element and to the reference antenna element of the BS array, respectively, x_p is the spacing between the pth antenna element and the reference antenna element of the BS array, and α is the difference between the tilt angle of the ULA at the BS and the AAoD of the wave transmitting from the pth antenna element and impinging on the cth cluster. Recently, the authors extended the parabolic wavefront in [79] into the 3D space and time domain [80]. The two-state Markov process and shadowing processes were used to capture the non-stationary properties in spatial and temporal domains.

Authors in [81] also proposed a WINNER-type massive MIMO channel model. Different from the model in [79], where the array non-stationarity was modeled using a two-state Markov process, the array non-stationarity in [81] was modeled by dividing the BS array into several sub-arrays. The length of each sub-array is determined by the stationary distance, which is defined by the coherence distance of visible clusters. The clusters corresponding to each sub-array were independently generated. A gradual share of clusters was obtained depending on the overlapped regions of adjacent sub-arrays. Instead of using the parabolic wavefront in [79], the spherical wavefront in [81] was accurately calculated based on the clusters' delays and angles.
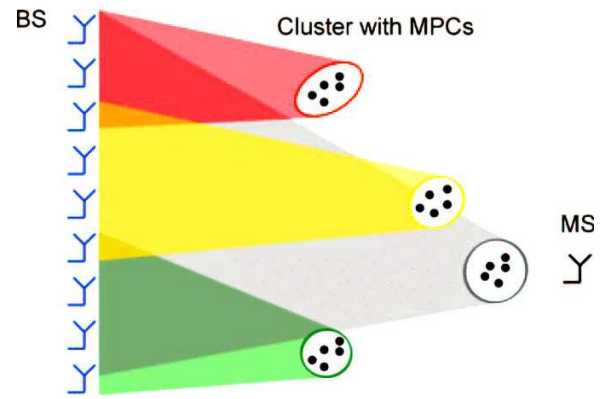
Authors in [82] and [83] proposed massive MIMO channel models based on COST 2100 channel model [84]. The array non-stationarity was modeled by introducing visibility region (VR) not only at the mobile station (MS) side (MS-VR), but also at the BS side (BS-VR). Different from the MS-VR, which acts on the temporal domain, the BS-VR acts on the array domain. As shown in Fig. 3, different BS-VRs are represented by different colors and they determine the visibility of different clusters over the large array. A cluster is active and contributes to the channel only when the MS is in its MS-VR and the BS antenna element is in its BS-VR. The spherical wavefront and variations of channel statistics over the large array were calculated from the geometry. Instead of using a birth-death process or 2D VR of antenna array, authors in [85] presented a 3D two-cylinder massive MIMO channel model. The array non-stationarity was modeled by assigning each antenna a 3D visible area, which is defined as a virtual sphere centered at each antenna element. A cluster can be "seen" by an antenna only when the cluster is located in the corresponding visible area, and thus each antenna has its own set of clusters.

Apart from GBSMs, authors in [86] and [87] developed massive MIMO channel models based on correlation-based stochastic models (CBSMs). In [88], a Kronecker-based stochastic model (KBSM) was developed for massive MIMO systems by introducing a birth-death process over the array. In [89], the authors proposed an empirical massive MIMO channel matrix model based on channel measurements. The channel matrix is represented as sum of a fixed matrix and a random matrix. The latter characterized the transmitting/receiving correlations and their coupling. In [90], a packet-level channel model based on a finite-state Markov chain (FSMC) was proposed for massive MIMO channels. Besides the aforementioned stochastic models, deterministic models such as ray-tracing (RT) model [91], ray-launching (RL) model [92], and map-based model [10] were also developed for massive MIMO channel modeling.

B. V2V Channel Models

Because of the unique propagation conditions, V2V channels exhibit very different propagation characteristics compared to the cellular communication channels [16]. In V2V

communications, both the transmitter and the receiver are relatively low and surrounded by a large number of scatterers. The transmitter and the receiver as well as scatterers could be moving, resulting in large Doppler shifts and making the channel non-stationary [11], [12]. Propagation environments such as highway and urban canyon can also make great impacts on channel characteristics. All above-mentioned propagation conditions have to be considered carefully in V2V channel modeling.

The early V2V channel models are 2D GBSMs, e.g., two-ring model [93]–[95]. The two-ring model assumes that the transmitter and receiver are surrounded by large numbers of local scatterers located on two regular rings. The statistical properties such as temporal autocorrelation function (ACF) and Doppler PSD can be derived with analytical solution from the geometry of the model. An improved two-ring model for V2V channels was proposed in [96]. The model took into account the LoS, single-bounced, and double-bounced components, making the model suitable for both micro- and macro-cells. By employing multiple scattering rings, the narrowband two-ring model was extended to wideband models [97], [98]. A further advance was presented in [99]–[101], where the authors proposed an adaptive V2V model by combining a two-ring model and an ellipse model. Through changing the power proportion of different propagation components, the model can be adapted to a wide range of V2V scenarios, e.g., macro-, micro-, and pico-cells. The LCR and AFD of the adaptive V2V model were derived in [102], where the obtained expressions can incorporate many existing LCRs and AFDs as special cases and fit the measurement results very well. Based on the multi-ring model, a cooperative MIMO channel model was proposed in [103]. By adjusting some key parameters, the proposed model can be adapted to a total of 12 mixed scenarios, i.e., 4 physical scenarios (macro-, micro-, pico-cells, and indoor scenarios) multiply by 3 application scenarios (BS, MS, and relay cooperation), and can capture the impacts of the local scatterers density on channel statistics. Other 2D regular-shaped GBSMs (RS-GBSMs) such as street scattering model [104], [105], T-Junction scattering model [106], [107], blind corner scattering model [108] were also adopted for modeling certain V2V channels. Statistical properties such as cross correlation function (CCF), ACF, and Doppler PSD can be derived from corresponding geometric relationships.

The 2D V2V models, which assume the waves propagate in the horizontal plane, are more suitable for certain scenarios, such as rural areas. However, in urban scenarios, the transmitter and receiver are closely located and waves can be diffracted and reflected off from high buildings. Therefore, wave propagations in both the horizontal and the vertical planes have to be considered. In [109], the authors proposed a 3D two-cylinder based V2V channel model, in which the scatterers were assumed to lie on the surfaces of two cylinders. The wideband version of the 3D two-cylinder model and its experimental verification can be found in [110]–[112]. In [113] and [114], the authors extended the work of [99] into a 3D non-stationary model, which combines the LoS component, a two-sphere model, and multiple confocal elliptic-cylinder models. The azimuth and elevation angles were described
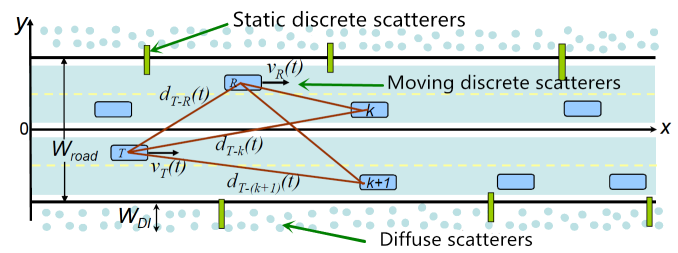

Fig. 4. A typical V2V propagation environment [121].

using the von Mises-Fisher distribution. The proposed 3D model was considered to be more general and realistic than 2D models and can be adapted to a wide range of V2V scenarios.

Further advances were proposed in [115]–[117], where V2V channel models were developed by taking into account both fixed scatterers and moving scatterers. Extra Doppler frequency shifts due to moving scatterers were considered. Few V2V models considered diffused scattering components, which can be stemmed from trees on the roadside [118]. Authors in [119] modeled the diffuse scattering using the low-complex multidimensional discrete prolate spheroidal sequences (DPSS). More general models were reported in [12], [120], and [121]. In Fig. 4, a typical V2V propagation environment is illustrated. The transmitter and receiver move in the same direction with the speeds of $v_T(t)$ and $v_R(t)$, respectively. An irregular-shaped GBSM (IS-GBSM) was developed by taking into account the LoS component, discrete components reflected from mobile scatterers, e.g., other vehicles, discrete components reflected from fixed scatterers, e.g., road signs and buildings, and diffuse components stemming from vegetation. By combining deterministic and stochastic approaches, the proposed models exhibit a good agreement with the measurement data and achieve a better trade-off between the accuracy and complexity compared to the traditional RS-GBSMs.

Non-geometrical stochastic models (NGSMs) such as tapped delay line (TDL) models were also used in V2V channel modeling. In TDL models, the channel impulse response (CIR) is represented by a linear finite impulse response (FIR) filter. Each tap of the TDL model is composed of several MPCs with non-resolvable delays. Tap weights are modeled by a random process with amplitudes following Rayleigh, Ricean, or Weibull distributions [122]. The early TDL-based V2V models were developed based on a series of measurements in cities and highways by Acosta-Marum and Ingram [123]–[126]. However, these models were based on the WSS assumption and cannot represent the non-stationarity of the V2V channels, which may lead to erroneous results in system performance prediction [127]. In [15], [128], and [129], non-stationary correlated scattering TDL channel models were proposed. In order to model the non-stationarity of V2V channels, parameters such as delays and powers were modeled as time-varying. The lifetime of the paths was modeled using a "persistence process", which is controlled by a first-order two-state Markov chain. Further data analysis illustrates that V2V channels fulfill neither WSS assumption, nor classical US assumption. The tap correlations of the models were
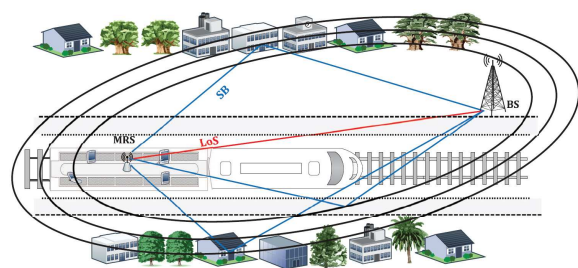
Fig. 5. A multiple confocal ellipses HST channel model [18].

provided based on measurement results. Benefitting from its simple structure, the computational complexity of TDL models is much less than the GBSMs. However, GBSMs are more versatile than the TDL models due to their complex geometric constructions which can represent realistic propagation environments by adjusting a large number of parameter configurations. A comprehensive comparison between GBSMs and TDL models for V2V channels was given in [121].

Deterministic models such as RT models were also adopted for V2V channel modeling. Early RT-based V2V models can be found in [130]–[133]. In [134], authors investigated the effects of antenna positions on the vehicles using a RT approach. By reconstructing virtual propagation environments and with the help of the GO and UTD theories, RT models can achieve a good agreement between the simulation and measurement results [135], [136]. Generally speaking, RT models can provide accurate and site-specific simulations but usually with large computational complexity.

C. HST Channel Models

HST scenario is assumed to be one of the typical scenarios for 5G systems [2], [137]. Considering the extremely high speed of train, e.g., 500 km/h, the future HST channel modeling has to address challenges such as non-stationarity, large Doppler shift [138], fast handover [139], and adapting to diverse HST propagation environments [140], including open space, viaduct, cutting, hilly terrain, tunnel, station, etc. Thus, HST scenario could be one of the most challenging scenarios in 5G channel modeling.

Most of the existing HST channel models were developed based on GBSMs. Authors in [141] proposed a one-sphere channel model for open space HST scenario. The scatterers were assumed to be located on the surface of a sphere with the train located at the center. A non-stationary wideband ellipse channel model for HST communication system was proposed in [18] and [142]. As shown in Fig. 5, scatterers were assumed to be located on multiple confocal ellipses with the transmitter and receiver located at two focal points. Waves reflected from the scatterers on the same ellipse arrive with the same delay. The non-stationarity of HST channel is caused by the time-varying distance between the transmitter and receiver. Time-varying angles of the model were calculated based on the geometry. The stationary interval was adopted to measure the stationarity of the HST channel model and compared with the measurement data. By using different scenario-specific parameters, the authors further extended the model in [142]

into a more general one [143], which can be applied to the three most common HST scenarios, i.e., open space, viaduct, and cutting scenarios. Authors in [144] proposed a GBSM that combined a one-ring model and an elliptical model for HST viaduct scenario. The channel parameters including the K-factor and Doppler PSD were obtained from channel measurements. A GBSM for HST cutting scenario was proposed in [145]. Channel parameters, including PLE and K-factor were extracted from measurement data. The cluster size was calculated based on cutting structure and channel parameters. A 3D cylinder-shape GBSM for HST tunnel scenario was proposed in [19] and [146]. The model considered both the single-bounced and multiple-bounced rays reflected from the scatterers randomly distributed on the inner walls of the tunnel. A new geometry-based random-cluster model for HST channels was proposed in [147]. The variations of delay and Doppler of clusters over time were represented based on the geometrical relationships among the BS, the moving HST carriage, and the railway. Cluster characteristics, including per-cluster path loss, shadow fading, delay, and Doppler spreads, were extracted from the measurement data. Standardized channel models such as the WINNER II [48] and IMT-Advanced [148] also presented respective channel models for the fast-moving scenarios based on extensive HST channel measurements. Using the same model framework for other scenarios, the WINNER II and IMT-Advanced models can support the HST speed up to 350 km/h. In [149], the IMT-Advanced channel model was extended to a 2D non-stationary HST channel model by considering moving clusters in propagation environments. The appearance and disappearance of clusters were modeled by a birth-death process and the parameters such as delay, power, and angles were updated according to the geometry. Similarly, a more realistic 3D non-stationary WINNER+ based channel model can be found in [150]. The extra Doppler frequencies caused by the moving clusters were considered. Statistical properties such as LCR, AFD, and stationary interval were derived and validated by the measurement data.

NGSMs capture the characteristics of HST channels in a fully stochastic manner instead of considering the geometrical construction of propagation environments. A measurement-based stochastic model for HST channels was reported in [151]. The HST propagation environment was divided into two regions, i.e., Region 1: the train is under the BS antennas, so called bottom area, and Region 2: the train is out of bottom areas but can still receive strong LoS paths. Analysis results show that propagations in Region 1 are mainly affected by the antenna radiation patterns. However, environment variations significantly influence propagations in Region 2. The proposed model took into account the impacts of directional BS antennas and characterized cell-to-cell variations of HST channels. Authors in [152] and [153] developed channel models for HST communication system based on FSMCs, providing an effective way to capture fast fading features of the HST channels. A position-based TDL model for HST communication system was proposed in [154]. Parameters such as K-factor, Doppler frequency, and delay spread were parameterized based on extensive HST channel measurements and modeled as
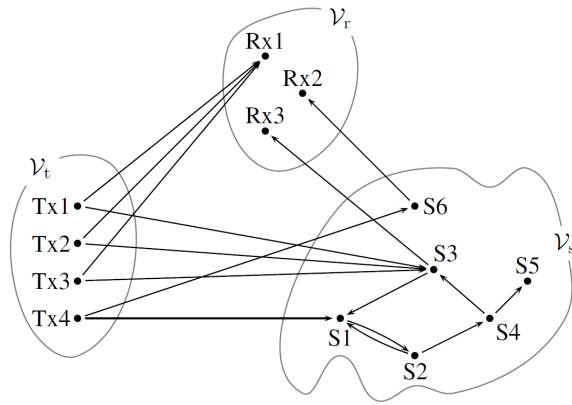
Fig. 6. A propagation graph with four transmit vertices, three receive vertices, and six scatterer vertices [157].

Fig. 7. Measured PDP where two TCs are composed of eight and six subpaths with a 25 ns minimum inter-cluster void interval [71].

functions of train position and transceiver separation. Based on the "on/off" TDL model in [128], authors in [155] modeled the dynamic behavior of multipath taps using a four-state Markov chain, i.e., no "births" or "deaths", only "births", only "deaths", and both "births" and "deaths". Similar method can be found in [156], where a second-order Markov process was used to describe the random "on/off" process of the multipath taps, e.g., "00" denotes the previous and present states are "off", "01" denotes the previous state is "off" and the present state is "on", etc. Authors in [158] developed a HST channel model using a propagation-graph modeling approach. As shown in Fig. 6, the local geographic details of environments were described by a random graph composed of a set of vertices (transmitter, receiver, and scatterers) and edges (propagation paths between vertices). The realization of CIR was generated by exhaustive searching for propagation paths connecting the transmitter and receiver. The proposed channel model can achieve specular-to-diffuse transition, which is difficult to acquire by the conventional RT models.

Deterministic channel models can provide a realistic and site-specific description of HST channels. A RT-based HST channel model was proposed in [159], where the propagation environment was reproduced by a concrete floor, two pairs of metallic railway tracks, several pairs of metallic pylons, and a concrete noise barrier on both sides of the track. Simulation results show that the Doppler spreads are reduced and the receive powers are increased when using directional antennas instead of omnidirectional antennas. In [160], a deterministic HST channel model was proposed which took into account all the transmission mechanisms existing in realistic HST propagation environments and considered the antenna influences including radiation pattern and polarization. The reflection and diffused scattering were modeled using a ray-optical approach, and the diffraction loss was predicted by a multi-edge diffraction model based on the raster database. A RT-based channel model focusing on composite HST scenario was proposed in [161]. The composite HST scenario was reconstructed by a 3D digital map. In general, deterministic modeling approaches are very suitable for modeling HST tunnel scenarios based on the regular scatterers distributed on tunnel walls. A multi-mode wa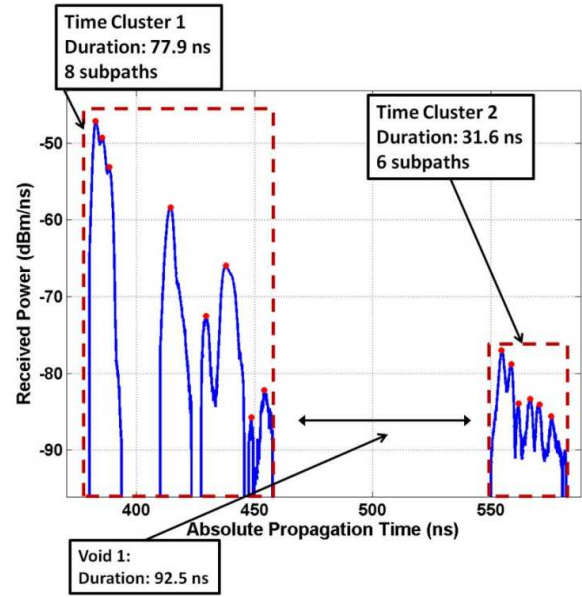veguide channel model for HST tunnel scenario was proposed in [162] by combining a GO model and a waveguide model. Statistics such as temporal ACF and PSD were derived.

D. mmWave Channel Models

A 3GPP-like mmWave channel model called statistical spatial channel model (SSCM) [71], [72], [163] was developed by Theodore S. Rappaport's team based on extensive mmWave channel measurements in the 28/38/60/73 GHz bands [5], [20], [55], [57], [164]–[169]. The SSCM extended the existing 3GPP model with higher temporal and spatial resolution properties using the time cluster-spatial lobe (TCSL) modeling method. The concepts of TC and SL are illustrated in Figs. 7 and 8. TCs are a number of MPCs with close delays to form a cluster, e.g., an inter-cluster void interval is larger than 25 ns, but can arrive from different directions. SLs indicate the set of arrival or departure rays whose powers continuously spread in the azimuth and elevation planes, e.g., at least -10 dB below the maximum power in the power azimuth spectrum (PAS), but could arrive over hundreds of nanoseconds. The concepts of TC and SL describe the temporal and spatial statistics independently, which are different from the cluster structure in the 3GPP/WINNER model. The CIR of the SSCM is the superposition of MPCs included in either a TC or a SL, and is given by

$$h_{\text{omni}}(t, \overrightarrow{\Theta}, \overrightarrow{\Phi}) = \sum_{n=1}^{N} \sum_{m=1}^{M_n} a_{m,n} e^{j\varphi_{m,n}} \cdot \delta(t - \tau_{m,n})$$
$$\cdot \delta(\overrightarrow{\Theta} - \overrightarrow{\Theta}_{m,n}) \cdot \delta(\overrightarrow{\Phi} - \overrightarrow{\Phi}_{m,n}) \quad (2)$$

where N and M_n are the number of TCs and the number of subpaths in the n-th TC, respectively, $a_{m,n}$, $\varphi_{m,n}$, and $\tau_{m,n}$ are the magnitude, phase, and delay of the m-th subpath in the n-th TC, respectively, $\overrightarrow{\Theta}_{m,n}$ and $\overrightarrow{\Phi}_{m,n}$ are the departure and arrival angle unit vectors, respectively.
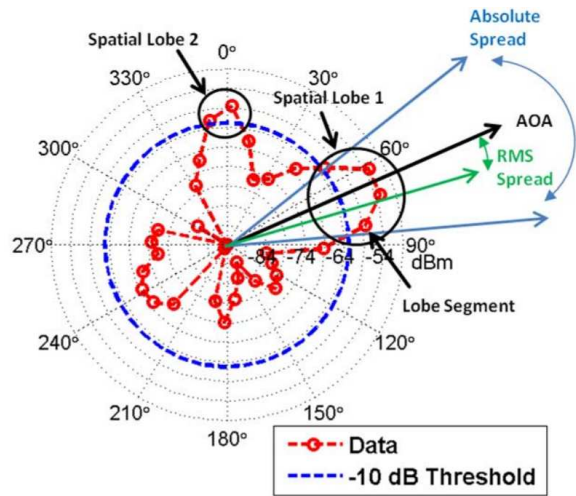
Fig. 8. Measured PAS where two SLs have a -10 dB power threshold [71].

Similar approaches can be found in [10], [73], and [170]–[173], where channel models were developed following the 3GPP/WINNER channel modeling approach and based on mmWave channel measurements and RT simulation results. It is worth noting that the massive MIMO channel measurements at 11, 16, 28, and 38 GHz in an indoor office environment were carried out in [23]. Statistical properties including APDP, power azimuth profile (PAP), power elevation profile (PEP), and RMS delay spread for the four mmWave bands were obtained. The massive MIMO propagation properties such as spherical wavefront, cluster birth-death, and parameter drifting over the antenna array at mmWave bands were validated and analyzed. Based on the measurement results, a non-stationary twin-cluster GBSM with a birth-death process was proposed.

NGSMs such as Saleh-Valenzuela (SV) model [174] are also popularly used in mmWave channel modeling due to its simple structure. The CIR of the SV model is given by

$$h(t) = \sum_{l=0}^{\infty} \sum_{k=0}^{\infty} \beta_{kl} e^{j\phi_{kl}} \delta(t - T_l - \tau_{kl}) \qquad (3)$$

where T_l denotes the delay of the l-th cluster, β_{kl}, ϕ_{kl}, and τ_{kl} are the amplitude, phase, and delay of the k-th arrival ray within the l-th cluster, respectively. The mmWave channel model in [175] was extended from the SV model by incorporating spatial information, which was assumed to be independent from delays. It was developed based on the measurement data at 7 GHz. The cluster arrival angles are uniformly distributed in the range $[0, 2\pi)$ and the azimuth AoAs (AAoAs) within a cluster are assumed to follow a zero-mean Laplacian distribution. A similar approach can be found in IEEE 802.15.3c channel model [176], where the SV model was extended by incorporating angular information based on the channel measurements between 57–64 GHz. A mmWave channel model for desktop environment was proposed in [177]. It was developed based on the measurements between 61–64 GHz. The model is a combination of a modified two-path model including the LoS path and a reflected path with random parameters, and a SV model representing NLoS components.

In [74], a series of channel measurements at 60 GHz were conducted in an indoor office environment. Parameters including power, delay, azimuth angle, and elevation angle were extracted using the SAGE algorithm and an extended SV-based model with angular information was developed. The authors found that the AAoDs have a wider distribution compared to the EAoDs and are significantly influenced by the antenna position and surrounding environments. However, EAoDs are more sensitive to the antenna height difference. More complicated 3D SV-based mmWave channel models with inter- and intra-cluster parameters for indoor environments were presented in IEEE 802.11ad channel model [64], [178]. The model was developed based on indoor channel measurements and RT simulation results at 60 GHz [65], [179]. Parameters such as delays and angles were described by specific probability density functions (PDFs). The clusters in IEEE 802.11ad model are composed of three components, i.e., central ray, pre-cursor rays, and post-cursor rays. The arrival rates of pre- and post-cursor rays were modeled as two Poisson processes and the average powers of rays were assumed to decay exponentially with delays, where the instantaneous powers are Rayleigh-distributed. An extension of the IEEE 802.11ad channel model was reported in [180]. The model takes into account the dependence of delay and angular domains. The spatial-temporal characteristics of clusters were modeled by two approaches, i.e., semi-deterministic approach based on RT and stochastic approach based on joint angular-delay PDFs. Measurement results at 60 GHz and 70 GHz revealed that the clustering behaviors are not significant in the angular-delay domain. Therefore, authors in [181] adopted a simpler structure instead of the cluster structure, which is widely used in IEEE 802.15.3c/802.11ad and 3GPP/WINNER models. The path angles were assumed to be uniformly distributed and the arrival of paths was modeled by a Poisson process. Besides, the model considers not only specular components, but also diffuse components which are more significant in mmWave bands than those in conventional bands. Other NGSMs such as the TDL channel model were also used in mmWave channel modeling. In [182], an indoor channel model for 60 GHz was proposed. The FIR filter coefficients were obtained based on wideband mmWave channel measurements. In [183], the TDL model for 27.4 GHz was extended by using random variable parameters and applied in the outdoor mmWave channel modeling.

Various mmWave channels in a wide range of scenarios have been parameterized and modeled using a deterministic method, i.e., RT method, such as urban area [184], [185], town square [186], indoor [187], [188], corridor [189], passenger cabin [190], HST [191], tunnel scenarios [192], etc. Apart from the RT approach, authors in [193]–[195] proposed deterministic mmWave channel models using a point cloud-based method, which can provide site-specific propagation predictions with high precision. The models were developed based on detailed environmental data, i.e., point cloud, which was obtained from laser scanning of investigated environment. The entire electromagnetic field was calculated through paths backscattering from the point cloud. Besides, some mmWave channel models were developed by combining deterministic

approaches and stochastic approaches. A semi-deterministic mmWave channel model for 3.8 and 60 GHz considering both specular components and diffuse components was proposed in [196]. The specular components were simulated through RT and the diffuse components were modeled by the graph theory. A similar channel model can be found in [197], where the RT-based model was extended by incorporating diffuse components using the effective roughness method. Recently, a unified propagation graph channel model for 60 GHz was proposed in [198], where the diffuse components were modeled by the semi-deterministic graph theory and the specular components were simulated by a single-lobe directive model.

E. Summary for Scenario-Specific 5G Channel Models

Table III shows the comparison of scenario-specific 5G channel models. Only part of the channel models were developed based on channel measurements. Since 5G channel models such as mmWave channel models heavily rely on measurement results, more channel measurements should be carried out for channel modeling. Besides, most of the existing channel models are GBSMs. Other modeling methods such as NGSM or methods combining multiple modeling approaches such as map-based hybrid method have also been considered.

IV. GENERAL 5G CHANNEL MODELS

In this section, we will introduce ten up-to-date general 5G channel models, which are COST 2100 channel model [84], [199], MiWEBA channel model [9], [200], QuaDRiGa [201], [202], mmMAGIC channel model [73], METIS channel model [10], 5GCMSIG [173], 3GPP channel model [203], IMT-2020 channel model [204], IEEE 802.11ay [205], and more general 5G channel model (MG5GCM) [206]. The "general" means the channel models can support various 5G communication technologies and can be adapted to different scenarios. All of these channel models, except MiWEBA and IEEE 802.11ay channel model, can be classified as GBSMs or adopted GBSMs since their primary modules root from SCM and WINNER II channel models. The grid-based GBSM (GGBSM) was first presented by METIS and then adopted by 5GCMSIG and mmMAGIC. It was developed in order to provide a smooth time evolution and spatially consistent simulations through interpolating channel parameters among the nearest grids in a 2D map. The deterministic modeling approach, i.e., map-based approach, proposed by METIS, was developed based on a simple 3D geometrical environment to provide an accurate and realistic channel data. The map-based hybrid model was first proposed by METIS and 3GPP, and then admitted by IMT-2020. It was developed by combining a GBSM and a map-based model. The map-based hybrid model can provide a flexible and scalable simulation, and at the same time can achieve a tradeoff between accuracy and complexity. Besides a GBSM and a map-based hybrid model, the IMT-2020 also proposed an extension module based on the time-spatial propagation (TSP) model [207]. It was used as an alternative modeling method to generate channel parameters by taking into account environment-specific parameters such as street width, building height, etc. Considering the quasi-optical characteristics of mmWave bands, the MiWEBA and IEEE 802.11ay proposed a quasi-deterministic (Q-D) modeling approach by combining the deterministic approach and the stochastic approach. The Q-D approach was reported to have the ability to meet the major challenges of outdoor channel modeling at 60 GHz.

A. COST 2100 Channel Model

COST 2100 channel model stems from COST 259 channel model [208] and COST 273 channel model [209]. It focuses on the frequency bands below 6 GHz. As shown in Fig. 9, there are three kinds of clusters in COST 2100 model, i.e., local clusters, single-bounced clusters, and twin clusters. Local clusters are situated around the BS or MS. Both single-bounced clusters and twin clusters are situated far away from BS and MS. The locations of single clusters can be determined by the delays and angular parameters at both sides. However, the locations of twin clusters have to be described respectively by both sides. All of the clusters in COST 2100 model are assumed to be dispersed in the propagation environment with fixed locations and shared by all links. Parameters like angles, delays, and powers were obtained based on the geometry and the distributions of cluster locations. This is contrary to the 3GPP/WINNER channel model, where clusters implicitly exist in the propagation environment and locations of clusters were indirectly determined by cluster parameters.

COST 2100 model inherits the concept of VR from COST 273 model. VRs were defined as identically sized circular regions and uniformly distributed in the azimuth plane. They indicate whether a cluster can be "seen" by the MS, that is, whether a cluster is active and how much it contributes to a channel realization. VRs can be overlapped and each VR corresponds to a specific cluster. As the MS enters and leaves different VRs, the corresponding clusters change, resulting in non-stationary channel simulations.

Benefitting from specific locations of clusters, the closely located receivers can see similar environments. Thus, the model can be simulated in a natural and realistic way and at the same time achieve spatial consistency. COST 2100 channel model supports smooth time evolution and long time/distance simulation. Furthermore, based on the fixed locations of clusters, spherical wavefronts can easily be obtained. Although COST 2100 model has many advantages, such as smooth time evolution, it is relatively difficult to extract and validate the cluster characteristics through channel measurements. Besides, the propagation environments represented by the three kinds of clusters and their VRs are relatively complex. Although the propagation environments were modeled in 3D, the VRs are still 2D. All of these limit the application of COST 2100 channel model.

B. MiWEBA Channel Model

The MiWEBA channel model can support frequency range between 57 and 66 GHz. Measurements in [5], [55], [64], and [210] illustrated that in mmWave propagations, the LoS and low-order reflection components constitute most of the

TABLE III
IMPORTANT SCENARIO-SPECIFIC 5G CHANNEL MODELS.

| Ref	Application	Modeling Approach	3D Modeling	Time Evolution	Wideband	Measurement Campaign*
[75], [80]	massive MIMO	IS-GBSM	yes	yes	yes	no
[79]	massive MIMO	IS-GBSM	no	yes	yes	no
[81]–[83]	massive MIMO	IS-GBSM	yes	yes	yes	yes
[76]–[78]	massive MIMO	RS-GBSM	no	yes	yes	no
[85]	massive MIMO	RS-GBSM	yes	no	no	no
[86], [88]	massive MIMO	NGSM	-	no	yes	no
[89]	massive MIMO	NGSM	-	no	no	yes
[87], [90]	massive MIMO	NGSM	-	no	yes	yes
[91]	massive MIMO	RT	yes	no	no	no
[92]	massive MIMO	RL	yes	no	no	yes
[93]–[96], [99], [101], [102], [108], [115], [117]	V2V	RS-GBSM	no	no	no	no
[97], [98], [100], [106], [107]	V2V	RS-GBSM	no	no	yes	no
[104]	V2V	RS-GBSM	no	yes	no	no
[105]	V2V	RS-GBSM	no	no	no	yes
[110], [111], [116]	V2V	RS-GBSM	yes	no	yes	no
[109], [113]	V2V	RS-GBSM	yes	no	no	no
[112]	V2V	RS-GBSM	yes	no	yes	yes
[114]	V2V	RS-GBSM	yes	yes	yes	no
[119]	V2V	IS-GBSM	no	no	no	yes
[12], [120]	V2V	IS-GBSM	no	yes	yes	yes
[118], [123]–[126]	V2V	NGSM	-	no	yes	yes
[15], [128], [129]	V2V	NGSM	-	yes	yes	yes
[130]–[134]	V2V	RT	yes	no	yes	no
[135], [136]	V2V	RT	yes	no	yes	yes
[141]	HST	RS-GBSM	yes	no	no	no
[18], [142], [143]	HST	RS-GBSM	no	yes	yes	no
[19], [146]	HST	RS-GBSM	yes	yes	yes	no
[144]	HST	RS-GBSM	no	no	no	yes
[145]	HST	IS-GBSM	yes	no	no	yes
[48], [147], [148]	HST	IS-GBSM	no	no	yes	yes
[149]	HST	IS-GBSM	no	yes	yes	no
[150]	HST	IS-GBSM	yes	yes	yes	no
[151], [153], [154], [158]	HST	NGSM	-	no	no	yes
[152]	HST	NGSM	-	no	no	no
[155], [156]	HST	NGSM	-	yes	yes	yes
[159]	HST	RT	yes	no	yes	no
[160], [161]	HST	RT	yes	no	yes	yes
[23], [71], [72], [163] [170], [171]	mmWave	IS-GBSM	yes	no	yes	yes
[64], [74], [175]–[178], [180]–[183]	mmWave	NGSM	-	no	yes	yes
[184]–[192]	mmWave	RT	yes	no	yes	no
[193]–[195]	mmWave	point cloud-based	yes	no	yes	yes
[196]–[198]	mmWave	semi-deterministic	yes	no	yes	yes
*: Measurement campaigns have been conducted before channel modeling						
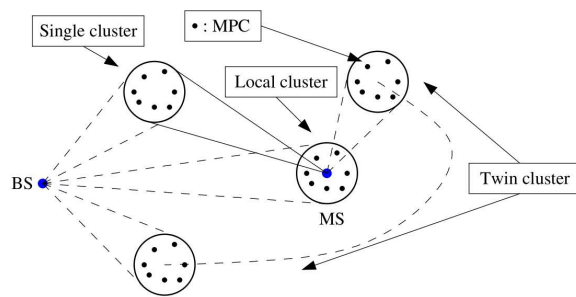
Fig. 9. Three kinds of clusters in COST 2100 channel model [84].

receiving power, whereas the power of diffraction components is relatively trivial. Considering the quasi-optical nature of

the propagation channels at mmWave bands, the MiWEBA channel model adopted a Q-D approach. As shown in Fig. 10, the CIR of the MiWEBA model is a superposition of D-rays and R-rays. The D-rays contribute to the major part of the received power and were modeled by a deterministic approach based on the geometry of the environment. The R-rays are weaker waves reflected from cars, trees, lampposts, benches, etc., and being described as random clusters with specified statistical parameters extracted from channel measurement data or RT simulation results.

The MiWEBA channel model supports several new communication technologies such as beamforming, massive MIMO communications, and D2D communications. It considers the ratio of diffusion to specular reflection components and supports time evolution. However, for the first version (D5.1),
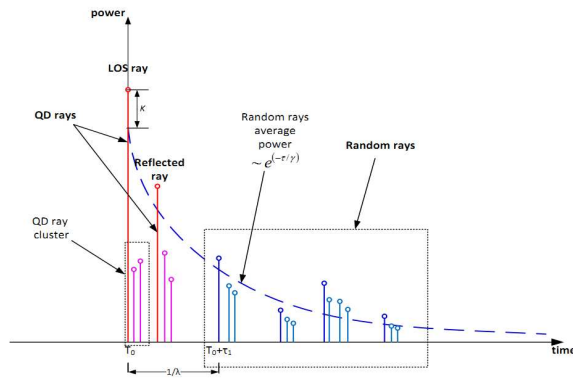
Fig. 10. CIR structure of MiWEBA model [9].

Fig. 11. Transitions between segments and obtaining the velocity variations by interpolation [201].

only three scenarios, i.e., outdoor access, backhaul/fronthaul, and D2D scenarios at 60 GHz band, were parameterized. The dynamic modeling ability of MiWEBA channel model is still very limited. The D-rays of MiWEBA model were obtained using the RT method based on a specific propagation environment.

C. QuaDRiGa

The QuaDRiGa is a GBSM evolved from WINNER+ channel model and was extended to support several new features [201]. The latest version of QuaDRiGa can support frequency range between 0.45 and 100 GHz. One of the improvements in QuaDRiGa is the generation process of correlated LSPs. The correlated maps in QuaDRiGa were generated by the means of 2D map covering all the locations of the receivers. Every pixels in the map were assigned with i.i.d. zero-mean Gaussian random variables [211]. In order to obtain a smooth location evolution of LSPs, the 2D maps were filtered with two additional FIRs formed based on the LSP correlation distance, not only in the horizontal and vertical directions, but also in the diagonal directions [201], [202]. The QuaDRiGa supports smooth time evolution for a long time/distance by separating the receiver trajectory into several segments. A segment can be considered as a time interval in which the LSPs do not change significantly and the WSS assumption is valid [48]. In each segment, a certain amount of clusters were generated independently and evolved with time based on the geometric relationships. As shown in Fig. 11, QuaDRiGa combined the independent segments into a long time sequence of channel coefficients using overlapping regions, in which old clusters ramp down and new clusters ramp up following a sine square function. By interpolating the channel coefficients non-uniformly, the QuaDRiGa can model the channels when the MS moves with an acceleration. The latest version of QuaDRiGa supports spatial consistency of both LSPs and SSPs. Clusters were generated using a 3D correlated random process determined by decorrelation distances, which means two closed located receivers can see similar cluster sets.

The QuaDRiGa supports 3D antenna modeling, massive MIMO antennas, multi-user, multi-cell, and multi-hop networks. However, dual-mobility is not supported in the current version. Furthermore, the QuaDRiGa only adopted the WINNER-like
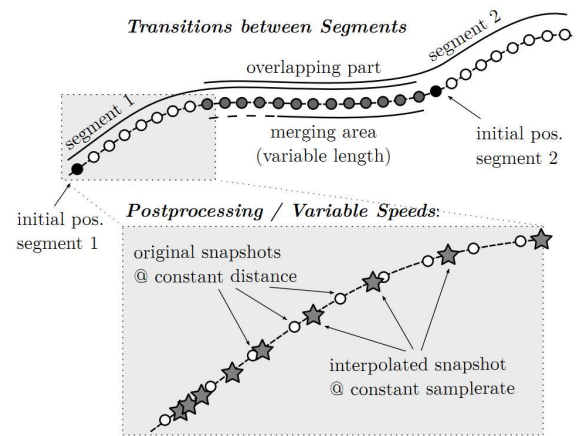
modeling framework. In order to support more advanced channel features and achieve a flexible and scalable simulation, combination with other modeling approach such as map-based model is necessary.

D. mmMAGIC Channel Model

The mmMAGIC channel model adopted the 3GPP 3D (3GPP TR36.873 [212]) channel modeling methodology and used the QuaDRiGa as a basis. A series of measurement campaigns conducted in various scenarios, e.g., indoor office, airport, urban micro (UMi) street canyon, UMi open square, and outdoor-to-indoor (O2I), and covering frequency bands between 6 GHz and 100 GHz provide measurement dada for modeling. In order to be eligible for mmWave bands, several new modeling approaches were proposed. The LSPs were modeled as frequency-dependent based on the measurement results. The clusters and rays were modeled using an extended SV model [174] characterising both spatial and temporal domains. The number of clusters and the number of rays within a cluster were modeled as random variables rather than fixed numbers. The arrival rates of clusters and rays were modeled as Poisson processes. Besides, blockage effects and ground reflection effects were also considered in the mmMAGIC model.

The mmMAGIC channel model supports a wide frequency range between 6 and 100 GHz and a large bandwidth of 2 GHz. It is presumed to meet most of the 5G channel model requirements. However, the dual-mobility is not yet supported and more scenarios need to be parameterized. Although the mmMAGIC channel model adopts a lot of advanced modeling components, how to achieve a flexible combination of those modeling components and reduce the complexity of the model should be addressed.

E. METIS Channel Model

In order to achieve a flexible and scalable channel modeling, METIS provided a map-based model, a stochastic model, and their combination, i.e., a hybrid model [10]. The stochastic

model and map-based model support frequency ranges up to 70 GHz and 100 GHz, respectively.

The map-based model was obtained based on a RT methodology and using a simplified 3D geometric description of a propagation environment and additional random shadowing objects. Propagation mechanisms including specular reflection, diffraction, diffuse scattering, and blocking were taken into account. Specular and diffuse components can be turned on or off to increase the accuracy or reduce the complexity. The map-based model is a promising candidate for 5G channel modeling, since it is claimed to meet most of the 5G channel model requirements and is suitable to validate 5G technologies such as mmWave communications, massive MIMO communications, and beamforming.

The stochastic model is a GBSM developed from the WINNER/3GPP model. In the case of D2D/V2V, both the transmitter and receiver are in motion, a six-dimensional (6D) correlation map of LSPs has to be used in order to generate spatially consistent LSPs, resulting in high computational complexity. The METIS proposes a novel sum of sinusoids approach to generate spatially consistent LSPs [213], [214], which is more efficient in computational and memory consumption than the traditional method. For the stochastic model illustrated in Fig. 12, an idea on time evolution and spherical wavefront was presented by fixing the locations of clusters based on the parameters like the delays and angles. Thus, the parameter drifts can be calculated according to the geometry.

Apart from the map-based model and stochastic model, the GGBSM was proposed for long time/distance simulations and achieves spatial consistence in the initial METIS channel models [215]. The GGBSM was obtained based on a 2D map covering all receiver locations. As illustrated in Fig. 13, the LSPs and SSPs were randomly generated for every pre-defined grid. The parameters at actual user locations were obtained by interpolating the parameters at the four nearest grids. The locations of clusters were determined through the delays and path angles, as illustrated in Fig. 12. Therefore, the drifting of LSPs and SSPs can be naturally traced based on the geometry.

The METIS channel model provides a flexible and scalable channel modeling framework and supports various scenarios such as dense urban macro (UMa) cell, UMi cell, indoor, shopping mall, D2D, and V2V links, with a wide range of frequencies. Although the map-based model is assumed to be less complex than the stochastic model, it is obtained from the simplified 3D digital map, which requires verification by measurements.

F. 5GCMSIG

The 5GCMSIG channel model was proposed by the special interest group (SIG) composed of several industrial and academic institutes. It can support a wide frequency range (0.5–100 GHz) and a large bandwidth (100 MHz for below 6 GHz and 2 GHz for above 6 GHz). Based on extensive measurements and RT simulations, the 5GCMSIG [173] extended the 3GPP 3D model to support higher frequency bands. The channel model includes path loss models, shadowing models, LoS probability, penetration models, preliminary fast fading
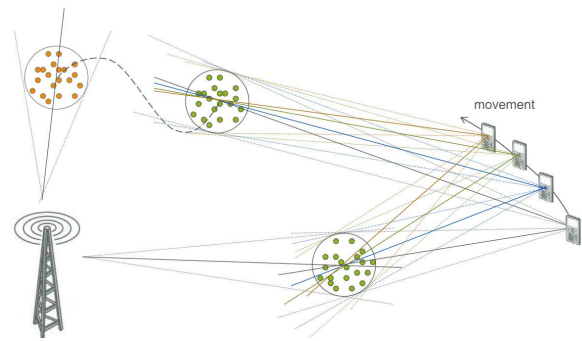

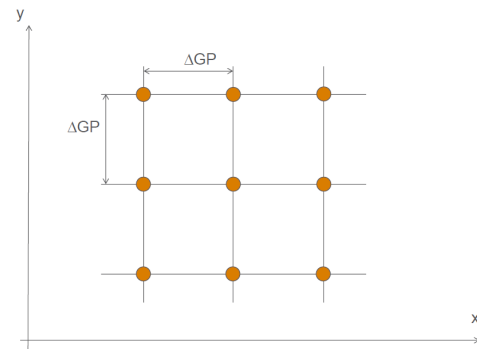Fig. 12.   Parameter drifting due to a small movement of the receiver [10].

Fig. 13.   Grid points separated by ΔGP in the xy plane [215].

models, and blockage models. Since having the same root of 3GPP/WINNER channel model, which does not support smooth time evolution and spatial consistency, the 5GCMSIG proposed three modeling methods to address these challenges, i.e., spatially consistent random variable method, geometric stochastic method, and grid-based method (similar to the METIS model [215]).

In spatially consistent random variable method, the random parameters including delay, shadowing, and offset of angles were generated by interpolating corresponding i.i.d. random parameters deployed in the simulation area. Similar method can be adopted to generate temporal/frequency consistent random parameters. The spatially consistent LoS/NLoS state was calculated through comparing a spatial consistency uniformly distributed random variable with the LoS probability at a specific location. The soft LoS/NLoS state was calculated through filtering spatially consistent binary LoS/NLoS state over the space. The spatially consistent indoor/outdoor state and soft indoor/outdoor state were calculated using the same steps.

In the geometric stochastic method, each cell was divided into several grids. In each of the grid, a set of LSPs were generated based on the specific PDFs [216]. MSs located in the same grid will have the same LSPs. The angles were updated according to the geometry using a linear approximation method [217]. The birth and death of clusters were modeled using a Poisson process. When the MS moves to the neighboring grid, the weakest cluster ramps down and the new cluster in the neighboring grid ramps up, which maintains the spatial consistency and keeps the number of clusters fixed.

The 5GCMSIG covers several new scenarios such as stadium, shopping mall, and street canyon. It provides smooth time evolution and spatially consistent simulations on both LSPs and SSPs. However, dual-mobility and spherical wavefront modeling are not yet supported. The 5GCMSIG provides different methods to achieve spatial consistency. How to evaluate those methods in different communication scenarios should be addressed in the future.

G. 3GPP Channel Model

The latest 3GPP channel model (3GPP TR38.901) [203] is the extension of the widely used 3GPP 3D channel model with several additional modeling components. It supports a wide frequency range (0.5–100 GHz) and a large bandwidth (up to 10% of carrier frequency).

In 3GPP channel model, the oxygen absorption at 53–67 GHz was modeled as a function of center frequency, delay, and 3D distance between the transmitter and the receiver. For large bandwidths and large antenna array, higher temporal and spatial resolutions were achieved. Specifically, the intra-cluster delays and powers in 3GPP model were determined unequally. Offset angles of rays within a cluster were generated randomly rather than using fixed values. That is, each MPC may have different delays, powers, and angles. Besides, the number of rays within a cluster was determined within a given range based on the parameters such as intra-cluster delay spread, intra-cluster angular spread, and array size. As for time evolution, powers, delays, and angles of clusters were updated according to the initial cluster parameters, MS moving velocity, and the initial location of the MS. Measurements in mmWave bands illustrate that a strong path reflected from ground superimposing with the LoS path can cause significant fading effects. Using a geometric method, the ground reflections were modeled as a separate component with the LoS component and NLoS components. Measurements indicate that mmWave channels are frequency dependent due to the interactions between propagation environments and the waves with significant different wavelengths [218]. In the 3GPP channel model, parameters such as delay spread, angular spread, and cluster power were modeled as frequency dependent. Moreover, it supports correlation modeling for multiple frequencies in the same scenario.

Besides the stochastic model, the 3GPP also proposed a map-based hybrid channel model, which is a combination of a stochastic component and a deterministic component. The stochastic component was mainly developed following the above-mentioned 3GPP stochastic modeling method. The deterministic component, as introduced in [10], was established using the RT method upon a digital map and considering the influences of environmental structures and materials. For the case of large bandwidth and massive MIMO, it separates the whole bandwidth into multiple sub-bands with bandwidths no more than c/D, i.e., the ratio of the speed of light to the maximum antenna aperture, and models the channel in respective sub-bands separately.

The 3GPP channel model considers spatial consistency, blockage effects, and atmosphere attenuation at mmWave
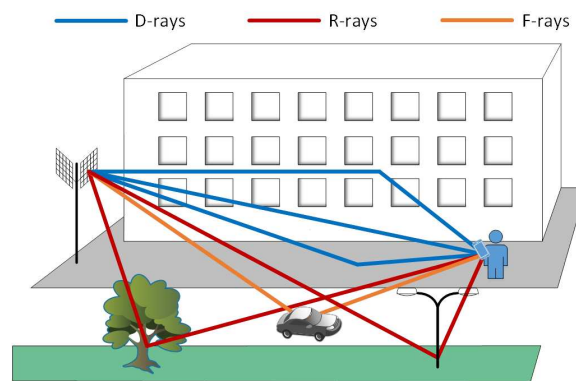

Fig. 14. D-rays, R-rays, and F-rays in IEEE 802.11ay channel model [205].

bands. However, the model has limited capabilities of simulating dual-mobility, antenna array non-stationarity, and spherical waves in massive MIMO. Besides, only four scenarios, i.e., street canyon, UMa cell, rural macro (RMa) cell, and indoor office, were parameterized.

H. IMT-2020 Channel Model

The IMT-2020 channel model [204] is a GBSM adopting the IMT-Advanced channel model [148] and 3GPP TR36.873 channel model [212] as a baseline and captures many new features such as supporting wide frequency range up to 100 GHz, large bandwidth, 3D propagation modeling, spatial consistency, large antenna array, blockage modeling, etc. For mmWave bands, the IMT-2020 channel model not only considered the gaseous absorption but also incorporated the vegetation effects, which are based on the fact that mmWave signals can be attenuated and diffusely scattered by leaves and diffracted around the canopy of trees. Similar to the 3GPP TR38.901, the IMT-2020 channel model proposed a ground reflection model and considered the frequency dependence of the channel. The cluster number in IMT-2020 channel model was modeled as a random number following the Poisson distribution with a mean value of 3 to 10.

The IMT-2020 channel model also proposed two extension modules, which provide alternative methods to generate channel parameters. The extension module below 6 GHz was developed based on the TSP model, which is an extension of IMT-Advanced TSP channel model. It took into account environment-specific parameters such as street width, building height, BS height, etc. The extension module above 6 GHz was developed based on the 3GPP map-based hybrid model, which provides an accurate and realistic simulation using a specific geometrical environment. However, dual-mobility simulation is not yet supported and only few scenarios have been parameterized.

I. IEEE 802.11ay Channel Model

The IEEE 802.11ay channel model [205] is an extension of IEEE 802.11ad channel model [64], which was developed for the 60 GHz band (57–68 GHz). It adopted the Q-D channel modeling approach inherited and extended from MiWEBA
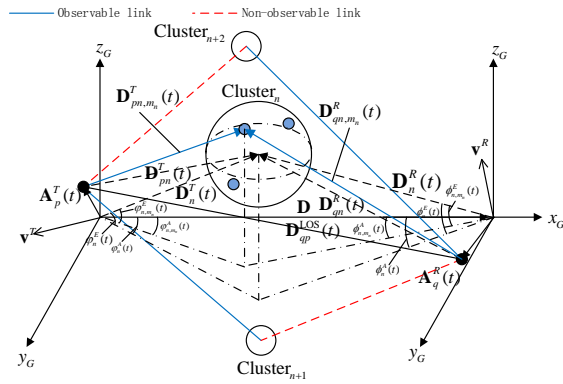
Fig. 15. A general 3D non-stationary 5G GBSM [206].

model [9], i.e., the multipath of IEEE 802.11ay model is composed of D-rays, R-rays, and F-rays. As is shown in Fig. 14, the D-rays is relatively strong rays such as the LoS ray, ground reflected ray, and other rays reflected from scenario-important objects. The D-rays were modeled as scenario-dependent. The R-rays are relatively week rays stemming from refections off small or random objects whose position cannot be estimated. The parameters of R-rays were modeled stochastically following certain distributions. Specifically, the amplitudes of R-rays were modeled as Rayleigh distributed, the phases of R-rays were as uniformly distributed, and the time of arrival follows a Poisson process. The F-rays stem from refections off moving objects such as vehicles, and only exist for relatively short durations. The F-rays were modeled stochastically similar to the method in R-rays but with shorter existence period.

The IEEE 802.11ad channel model is a SISO model and only concentrated on indoor scenarios, i.e., conference room, cubicle environment, and living room. The IEEE 802.11ay channel model extended the IEEE 802.11ad model by providing MIMO usage. Based on the RT and measurement results, the IEEE 802.11ay channel model covers more scenarios, such as street canyon and open area. In most outdoor scenarios, the D-rays, which contribute most to the propagation, are composed of two components, i.e., the LoS ray and ground reflected ray. However, the massive MIMO and high-mobility are not supported.

J. MG5GCM

Recently, a more general 3D non-stationary 5G channel model was proposed in [206]. The model can capture certain characteristics of key 5G communication scenarios including massive MIMO, HST, V2V, and mmWave communication secnarios. As shown in Fig. 15, the proposed model was developed based on the WINNER II and SV models. The array-time cluster evolution, i.e., clusters appearance and disappearance on the time axis and array axis, were modeled as birth-death processes. At each time instant, for new generated clusters, the delays, powers, and angles were randomly generated based on certain distributions. For survived clusters, parameters were updated according to their geometrical relationships. The

spherical wavefront was calculated according to the physical location of clusters in order to support massive MIMO communications. Considering the high temporal and spatial resolution requirements of mmWave channel models, delays and powers of rays within clusters were modeled unequally and the numbers of rays within clusters were modeled as Poisson distributed random variables. Besides, Doppler frequencies at both sides were considered in order to support V2V communications.

The MG5GCM combined several advanced channel modeling technologies, such as array-time evolution, spherical wavefront, intra-cluster delay spread, etc. It can meet most of the 5G channel modeling requirements and at the same time maintain the computational complexity relatively low. By setting parameters properly, the model can be adapted to various communication scenarios or reduced into various simplified channel models. However, the MG5GCM only concentrated on small-scale fading and neglected large-scale fading. Besides, parameters of the model for different scenarios need to be extracted from future channel measurements.

K. Comparison of General 5G Channel Models

Most of the general 5G channel models including QuaDRi-Ga, mmMAGIC channel model, METIS channel model, 5GCMSIG, 3GPP TR38.901 channel model, IMT-2020 channel model, and MG5GCM adopted the WINNER-like framework and extended it with additional modeling components to meet the 5G channel modeling requirements. In order to achieve a flexible and scalable simulation, the map-based hybrid channel model was also adopted by the METIS channel model, 3GPP TR38.901 channel model, and IMT-2020 channel model. Similar approach combining stochastic method and deterministic method called Q-D based model was proposed by MiWEBA and IEEE 802.11ay channel model. Most of the general 5G channel models support an extremely wide frequency range, e.g., from 0.45–100 GHz. Note that the MiWEBA and IEEE 802.11ay channel model only concentre on 60 GHz bands. For mmWave channel modeling, the MiWEBA channel model, IEEE 802.11ay channel model, 3GPP TR38.901 channel model, mmMAGIC channel model, IMT-2020 channel model, and the map-based channel model considered the blockage and gaseous absorption effects, which can exert a great influence on the propagation at mmWave bands. Besides, only the MG5GCM can support the four most challenging scenarios of 5G systems, i.e., massive MIMO communications, V2V communications, HST communications, and mmWave communications. A comprehensive comparison of the above-mentioned general 5G channel models is shown in Table IV.

V. FUTURE RESEARCH DIRECTIONS FOR 5G AND B5G CHANNEL MEASUREMENTS AND MODELS

Apart from the above-mentioned topics, there are still many debates over the specifications of future channel measurements and models. Most future researches will focus on developing channel models which are more efficient (combining multiple modeling approaches), covering extremely wide frequency

TABLE IV
COMPARISON OF GENERAL 5G CHANNEL MODELS.

Feature	COST 2100	MiWEBA	QuaDRiGa	METIS		5GCMSIG	3GPP	mmMAGIC	IMT-2020	IEEE 802.11ay	MG5GCM
Modeling approach	GBSM	Q-D based model	GBSM	stochastic	map-based	GBSM, GGBSM	GBSM, map-based hybrid model	GBSM, GGBSM	GBSM, TSP, map-based hybrid model	Q-D based model	GBSM
Frequency range (GHz)	<6	57-66	0.45-100	up to 70	up to 100	0.5-100	0.5-100	6-100	0.5-100	57-68	-
Bandwidth	-	2.16 GHz	1 GHz	100 MHz (< 6 GHz), 1 GHz @ 60 GHz	10 % of the center frequency	100 MHz (< 6 GHz), 2 GHz (> 6 GHz)	10 % of the center frequency	2 GHz	100 MHz (< 6GHz), 10% of the center frequency (> 6 GHz)	2.64 GHz	-
Support large array	-	yes	yes	no	yes	limited	yes	yes	yes	no	yes
Support spherical waves	no	yes	yes	no	yes	no	no	yes	no	no	yes
Support dual-mobility	no	yes	no	limited	yes	no	no	no	no	yes	yes
Support 3D (elevation)	yes	yes	yes	yes	yes	yes	yes	yes	yes	yes	yes
Support mmW	no	yes	yes	partly	yes	yes	yes	yes	yes	yes	yes
Dynamic modeling	yes	limited	yes	no	yes	yes	yes	yes	yes	limited	yes
Spatial consistency	yes	yes	yes	shadow fading only	yes	yes	yes	yes	yes	no	no
High mobility	yes	no	yes	limited	no	yes	limited	yes	limited	no	yes
Blockage modeling	no	yes	no	no	yes	yes	yes	yes	yes	yes	no
Gaseous absorption	no	yes	no	no	yes	no	yes	yes	yes	yes	no

-: There is no information in the related documents

bands (e.g., terahertz (THz) spectrum and visible light spectrum), concentrating on new scenarios (e.g., tunnel, underground, underwater, and even human body), and combining with other disciplines (e.g., big data and machine learning).

A. Combining Multiple Modeling Approaches

One of the future research directions is combining different kinds of channel models, such as GBSMs, NGSMs, and deterministic models. GBSMs assume that scatterers are distributed on geometric shapes. By adjusting a large number of parameters, it is relatively easy to fit the statistical properties to measurement data. The deterministic channel models, such as RT models, usually provide accurate and site-specific predictions with high computational complexity. In [10], the METIS proposed a hybrid channel model, which is composed of a stochastic model, i.e., GBSM and a deterministic model, i.e., map-based model. LSPs including path loss and shadowing were obtained from the map-based model, while the GBSM generated the SSPs. The METIS hybrid channel model provides a flexible and scalable channel modeling method and aims to achieve a tradeoff between accuracy and computational complexity.

The CBSMs are usually used to evaluate the performance of massive MIMO systems due to their low complexity. However, compared with GBSMs, the capability of spatial determinism of CBSMs is very limited. In [86], a statistical block fading channel model for multiuser massive MIMO system was proposed. The model is able to capture the time/frequency correlation as a CBSM and at the same time incorporated

spatial variations of massive channels as a GBSM. Recently, a hardware channel emulator was implemented by combining a improved WINNER+ channel model and the sum-of-frequency-modulation (SoFM) method [219]. Generally speaking, the number of hybrid channel models in the literature is very limited. How to combine different kinds of channel models and take accuracy and efficiency into consideration requires further investigation.

B. THz Communication Channel Modeling

The THz spectrum, ranging from 0.3 to 10 THz, lies between mmWave and infrared lightwaves in the electromagnetic spectrum. THz spectrum is considered as a new spectrum resource and has not been fully exploited [220]. However, because of the increasing demands for high speed wireless access and the progress of semiconductor devices, THz communication technologies have drawn increasing attention of researchers. Benefitting from the large bandwidth, THz communication is expected to provide a data rate of 100 Gbps or even higher [221]. However, due to the high frequency bands, signals propagate at THz can experience much larger free space path loss and atmosphere attenuation than those in microwave frequency bands [222]. Therefore, the THz communication system is most likely used in indoor environments combined with beam-steering techniques. The THz channel modeling is still in its preliminary phase and only few THz channel models have been developed. Authors in [223] proposed a GBSM for THz channels, which can be used to investigate the physical characteristics of the THz

channels and evaluate the system-level performance. A multi-ray THz channel model based on RT techniques was proposed and analyzed in [224], where the LoS, reflected, scattered, and diffracted components were taken into account. More THz channel models need to be developed in the future.

C. Visible Light Communication (VLC) Channel Modeling

Another promising spectrum resource receiving researchers' attention is visible light spectrum. The visible light lies in the electromagnetic spectrum ranging from 430 THz to 790 THz, where the waves can be perceived by human eye [225]. With the existing light emitting diode (LED) as source transmitter, VLC can provide illumination and communication simultaneously. VLC is considered as a promising supplement to the current microwave-based communications and has many attractive features. It is environment-friendly, energy-efficient, economical, and highly-secure [2]. Compared to the channels in microwave bands, VLC channels may exhibit much different characteristics [226]. However, up to now, only few VLC channel models have been developed. In [227] and [228], authors proposed deterministic models for VLC channels based on RT approach. In [229], authors proposed a geometry based single-bounced (GBSB) channel model for VLC channels based on a one-ring model. A more complicated geometry based multiple-bounced (GBMB) model for VLC channels was reported in [230]. The model was developed by combining a two-ring model and an ellipse model. Up to three-order reflections were considered in this model. A path loss channel model for VLC in underground mine scenario was reported in [231]. A comprehensive review of channel measurements and models for optical wireless communications can be found in [232]. More channel measurements and models for VLC channels are required in the future.

D. Molecular Communication Channel Modeling

Molecular communication is an emerging nanoscale communication technology and has a vast application prospect in biomedical, industrial, and military fields. Different from the traditional communication technology, molecular communication uses artificial cells, biomedical implants, or nanorobots as transmitter and receiver, and conveys manmade messages through exchanging molecules. Signal molecules propagate from the transmitter to the receiver in a variety of ways such as free space diffusion, molecular motor transfer, and nano-tube delivery. Different messages are distinguished by certain molecular patterns such as molecular concentration, molecular type, and release time. Up to now, the number of publications focusing on molecular channel modeling is very limited. Authors in [233] and [234] derived the channel capacity of molecular communication channels from the traditional mutual information formula. A linear channel model for intra/inter-cellular Ca^{2+} molecular communications was proposed in [235], where the end-to-end channel model was composed of three components, i.e., Ca^2+ wave generation, intercellular propagation, and intracellular propagation. The bit error probability was obtained based on the proposed channel model. A general channel model for molecular communications called N3Sim was reported in [236]. N3Sim is a simulation framework for diffusion-based molecular communications. The diffusion of molecules was simulated as Brownian motion in a fluid medium. The molecules inertia and collisions were considered in the proposed model. The molecular communication channel modeling has been studied in the literature for only about ten years and more realistic molecular communication channel models are required in the future.

E. Channel Modeling for Special/Extreme Scenarios

5G networks should provide a seamless coverage over a wide range of scenarios. However, some special or extreme scenarios, such as tunnel, unmanned aerial vehicle (UAV), underground, underwater/sea, fire communication secnarios, etc., were rarely considered in the current channel modeling. In general, modeling of these scenarios strongly depend on the corresponding channel measurements due to their unique environments and distinct propagation properties. For example, in tunnel scenarios, the propagation environment is usually a long enclosure space with circular- or rectangular-shaped cross section with rough interior walls. The waveguide effects caused by the limited space can have a great effect on wave propagation. The channels for tunnel scenarios can be modeled by various approaches, such as waveguide approach [237], full-wave approach [238], finite-state Markov approach [239], and geometry-based stochastic approach [146]. Unlike any other existing wireless communications, the UAV communication is the first communication technology that takes full advantage of the 3D propagation space, which means both the horizontal and vertical domains should be taken into account in the UAV channel modeling. Since UAVs fly above buildings and trees, the propagations between the air and ground are more likely to be the LoS propagations. As the propagation distance becomes larger, the LoS component can be blocked by obstacles such as trees and buildings and attenuates rapidly due to earth curvature [240]. Up to now, only a few channel measurements concentrated on UAV channels [241]–[244]. UAV channels can be modeled using different approaches, such as deterministic models [245], [246], NGSMs [247], [248], and GBSMs [249], [250]. Another topic receiving increasing attention is underground channel measurement and modeling. In underground environments, the irregularity and roughness of interior walls can severely attenuate the propagations, resulting in a larger value of PLE than that in indoor environments [251]. Besides, soil texture, moisture, depth, and distance between transmitter and receiver can also impact the propagations in underground environments [252]. The underground channel modeling heavily relies on the distinct propagation properties, which have to be extracted from extensive channel measurements. In the future, more channels in special/extreme scenarios should be measured and the propagation properties in those scenarios require further investigation.

F. Channel Modeling Based on Big Data Theories

The channel measurement is an essential step of 5G channel modeling. Considering the wide frequency range, huge bandwidth, large number of antennas, and diverse scenarios, the volume of measurement data can be very large. Measurement data processing is usually a time-consuming process and requires great computational power [253], [254]. Analysis results indicate that measurement data exhibits strong correlation in multiple dimensions, such as time, space, frequency, etc. Note that significant achievements in big data research field have been obtained in recent years. It is reasonable to develop channel models by taking advantage of big data theories, such as data mining and machine learning. In [255], the authors proposed a cluster-nuclei based channel model based on big data theories. The cluster-nuclei was defined as a cluster dominated in the CIR in diverse scenarios and can correspond to the propagation environment with a certain shape. Channel parameters were trained using a neural network provided by measurement data. The CIR can be generated with a limited number of cluster-nuclei. In general, the interdisciplinary research of big data and channel modeling is still in a preliminary phase and can gain more attentions with the development of big data theories.

VI. CONCLUSIONS

This paper has provided a comprehensive review of key topics in 5G channel measurements and modeling. Requirements for the 5G channel modeling have been provided. Existing channel measurements and models for the most challenging communication scenarios in 5G systems, i.e., massive MIMO communication, V2V communication, HST communication, and mmWave communication, have been reviewed and discussed. General channel models covering more 5G scenarios have been introduced and a comparison of these models has been provided. Future research directions for 5G and B5G channel measurements and models have been outlined. The 5G channel models should simulate wireless propagation channels over an extremely wide frequency range, covering various network topologies, and can be adapted to a great number of scenarios. In the future, multiple channel modeling approaches or hybrid channel modeling approaches rather than one modeling approach may be adopted, in order to address all the challenges caused by 5G systems and at the same time, achieve a good trade-off between model accuracy and complexity.

APPENDIX

List of Abbreviations

2D	two-dimensional
3D	three-dimensional
4G	fourth generation
5G	fifth generation
5GCM	5G Channel Model
6D	six-dimensional
AAoA	azimuth angle of arrival
AAoD	azimuth angle of departure
AASA	azimuth angular spread of arrival
ACF	temporal autocorrelation function
AFD	average fade duration
APDP	averaged power delay profile
APS	angular power spectrum
B5G	beyond 5G
BS	base station
CBSM	correlation-based stochastic model
CCF	cross correlation function
CIR	channel impulse response
CMD	correlation matrix distance
COST	European COoperation in the field of Scientific and Technical research
D2D	device-to-device
DPSS	discrete prolate spheroidal sequences
EAoD	elevation angle of departure
EASA	elevation angular spread of arrival
FCF	frequency correlation function
FIR	finite impulse response
FSMC	finite-state Markov chain
GBMB	geometry based multiple-bounced
GBSB	geometry based single-bounced
GBSM	geometry-based stochastic model
GGBSM	grid-based geometry-based stochastic model
GO	geometrical optics
GTD	geometric theory of diffraction
HST	high-speed train
i.i.d.	independent and identically distributed
IS-GBSM	irregular-shaped geometry-based stochastic model
KBSM	Kronecker-based stochastic model
LA	linear array
LCR	level crossing rate
LED	light emitting diode
LoS	line-of-sight
LRS	local region stationarity
LSP	large-scale parameter
METIS	Mobile and wireless communications Enablers for the Twenty-twenty Information Society
MG5GCM	more general 5G channel model
MIMO	multiple-input multiple-output
MiWEBA	Millimeter-Wave Evolution for Backhaul and Access
mmMAGIC	mm-wave based Mobile radio Access network for fifth Generation Integrated Communications
mmWave	millimeter wave
MPC	multipath component
MS	mobile station
NGSM	non-geometrical stochastic model
NLoS	non line-of-sight
O2I	outdoor-to-indoor
PAP	power azimuth profile
PAS	power azimuth spectrum
PDF	probability density function
PDP	power delay profile
PEP	power elevation profile

PLE	path loss exponent
PSD	power spectrum density
Q-D	quasi-deterministic
QuaDRiGa	QUAsi Deterministic RadIo channel GernerAtor
RA	rectangular array
RDA	rotated directional antenna
RL	ray-launching
RMS	root-mean-square
RS-GBSM	regular-shaped geometry-based stochastic model
RT	ray-tracing
SA	spherical array
SAGE	space-alternating generalized expectation-maximization
SCM	spatial channel model
SIG	special interest group
SoFM	sum-of-frequency-modulation
SSCM	statistical spatial channel model
SSP	small-scale parameter
SV	Saleh-Valenzuela
TCSL	time cluster-spatial lobe
TDL	tapped delay line
THz	terahertz
TSP	time-spatial propagation
UAV	unmanned aerial vehicle
UCA	uniform cylindrical array
ULA	uniform linear array
UMa	urban macro
UMi	urban micro
URA	uniform rectangular array
US	uncorrelated scattering
UTD	uniform theory of diffraction
UVA	uniform virtual array
V2V	vehicle-to-vehicle
VLC	visible light communication
VNA	vector network analyzer
VR	visibility region
WSS	wide-sense stationary

REFERENCES

[1] F. Boccardi, R. W. Heath, A. Lozano, T. L. Marzetta, and P. Popovski, "Five disruptive technology directions for 5G," *IEEE Commun. Mag.*, vol. 52, no. 2, pp. 74–80, Feb. 2014.

[2] C.-X. Wang, F. Haider, X. Gao, X. H. You, Y. Yang, D. Yuan, H. M. Aggoune, H. Haas, S. Fletcher, and E. Hepsaydir, "Cellular architecture and key technologies for 5G wireless communication networks," *IEEE Commun. Mag.*, vol. 52, no. 2, pp. 122–130, Feb. 2014.

[3] P. Popovski *et al.*, METIS, ICT-317669/D1.1, "Scenarios, requirements and KPIs for 5G mobile and wireless system," Apr. 2013.

[4] W. Roh, J. Y. Seol, J. Park, B. Lee, J. Lee, Y. Kim, J. Cho, K. Cheun, and F. Aryanfar, "Millimeter-wave beamforming as an enabling technology for 5G cellular communications: Theoretical feasibility and prototype results," *IEEE Commun. Mag.*, vol. 52, no. 2, pp. 106–113, Feb. 2014.

[5] T. S. Rappaport, S. Sun, R. Mayzus, H. Zhao, Y. Azar, K. Wang, G. N. Wong, J. K. Schulz, M. Samimi, and F. Gutierrez, "Millimeter wave mobile communications for 5G cellular: It will work!" *IEEE Access*, vol. 1, pp. 335–349, May 2013.

[6] S. Kutty and D. Sen, "Beamforming for millimeter wave communications: An inclusive survey," *IEEE Commun. Surveys Tut.*, vol. 18, no. 2, pp. 949–973, Secondquarter 2016.

[7] E. G. Larsson, O. Edfors, F. Tufvesson, and T. L. Marzetta, "Massive MIMO for next generation wireless systems," *IEEE Commun. Mag.*, vol. 52, no. 2, pp. 186–195, Feb. 2014.

[8] F. Rusek, D. Persson, B. K. Lau, E. G. Larsson, T. L. Marzetta, O. Edfors, and F. Tufvesson, "Scaling up MIMO: Opportunities and challenges with very large arrays," *IEEE Signal Process. Mag.*, vol. 30, no. 1, pp. 40–60, Jan. 2013.

[9] A. Maltsev *et al.*, MiWEBA, FP7-ICT-608637/D5.1 "Channel modeling and characterization," V1.0, Jun. 2014.

[10] V. Nurmela *et al.*, METIS, ICT-317669/D1.4, "METIS Channel Models," Jul. 2015.

[11] I. Tan, W. Tang, K. Laberteaux, and A. Bahai, "Measurement and analysis of wireless channel impairments in DSRC vehicular communications," in *Proc. IEEE ICC'08*, Beijing, China, May 2008, pp. 4882–4888.

[12] O. Renaudin, V. M. Kolmonen, P. Vainikainen, and C. Oestges, "Wideband measurement-based modeling of inter-vehicle channels in the 5 GHz band," *IEEE Trans. Veh. Technol.*, vol. 62, no. 8, pp. 3531–3540, Oct. 2013.

[13] C.-X. Wang, S. Wu, L. Bai, X. You, J. Wang, and C.-L. I, "Recent advances and future challenges for massive MIMO channel measurements and models," *Sci. China Inf. Sci, Invited Paper*, vol. 59, no. 2, pp. 1–16, Feb. 2016.

[14] K. Zheng, S. Ou, and X. Yin, "Massive MIMO channel models: A survey," *Int. J. Antennas Propag.*, vol. 2014, no. 11, pp. 1–10, 2014.

[15] D. W. Matolak, "Channel modeling for vehicle-to-vehicle communications," *IEEE Commun. Mag.*, vol. 46, no. 5, pp. 76–83, May 2008.

[16] A. F. Molisch, F. Tufvesson, J. Karedal, and C. F. Mecklenbrauker, "A survey on vehicle-to-vehicle propagation channels," *IEEE Wireless Commun.*, vol. 16, no. 6, pp. 12–22, Dec. 2009.

[17] C.-X. Wang, X. Cheng, and D. I. Laurenson, "Vehicle-to-vehicle channel modeling and measurements: recent advances and future challenges," *IEEE Commun. Mag.*, vol. 47, no. 11, pp. 96–103, Nov. 2009.

[18] C.-X. Wang, A. Ghazal, B. Ai, Y. Liu, and P. Fan, "Channel measurements and models for high-speed train communication systems: A survey," *IEEE Commun. Surveys Tuts.*, vol. 18, no. 2, pp. 974–987, 2nd Quart., 2016.

[19] Y. Liu, A. Ghazal, C.-X. Wang, X. Ge, Y. Yang, and Y. Zhang, "Channel measurements and models for high-speed train wireless communication systems in tunnel scenarios: A survey," *Sci. China Inf. Sci.*, vol. 60, no. 10, Oct. 2017.

[20] T. S. Rappaport, G. R. MacCartney, M. K. Samimi, and S. Sun, "Wideband millimeter-wave propagation measurements and channel models for future wireless communication system design," *IEEE Trans. Commun.*, vol. 63, no. 9, pp. 3029–3056, Sept. 2015.

[21] S. Payami and F. Tufvesson, "Channel measurements and analysis for very large array systems at 2.6 GHz," in *Proc. EUCAP'12*, Prague, Mar. 2012, pp. 433–437.

[22] J. Chen, X. Yin, X. Cai, and S. Wang, "Measurement-based massive MIMO channel modeling for outdoor LoS and NLoS environments," *IEEE Access*, vol. 5, no. 99, pp. 2126-2140, 2017.

[23] J. Huang, C.-X. Wang, R. Feng, J. Sun, W. Zhang, and Y. Yang, "Multi-frequency mmWave massive MIMO channel measurements and characterization for 5G wireless communication systems," *IEEE J. Sel. Areas Commun.*, vol. 35, no. 7, pp. 1591–1605, Jul. 2017.

[24] X. Gao, F. Tufvesson, O. Edfors, and F. Rusek, "Measured propagation characteristics for very-large MIMO at 2.6 GHz," in *Proc. ASILOMAR'12*, Pacific Grove, CA, Nov. 2012, pp. 295–299.

[25] X. Gao, O. Edfors, F. Rusek, and F. Tufvesson, "Massive MIMO performance evaluation based on measured propagation data," *IEEE Trans. Wireless Commun.*, vol. 14, no. 7, pp. 3899–3911, Jul. 2015.

[26] À. O. Martínez, E. De Carvalho, and J. Ø. Nielsen, "Towards very large aperture massive MIMO: a measurement based study," in *Proc. IEEE GC Wkshps'14*, Austin, TX, Dec. 2014, pp. 281–286.

[27] D. W. Matolak, I. Sen, W. Xiong, and N. T. Yaskoff, "5 GHz wireless channel characterization for vehicle to vehicle communications," in *Proc. IEEE MILCOM'05*, Atlantic City, NJ, Oct. 2005, pp. 3016–3022.

[28] L. Cheng, B. E. Henty, D. D. Stancil, F. Bai, and P. Mudalige, "Mobile vehicle-to-vehicle narrow-band channel measurement and characterization of the 5.9 GHz dedicated short range communication (DSRC) frequency band," *IEEE J. Sel. Areas Commun.*, vol. 25, no. 8, pp. 1501–1516, Oct. 2007.

[29] R. He, A. F. Molisch, F. Tufvesson, Z. Zhong, B. Ai, and T. Zhang, "Vehicle-to-vehicle propagation models with large vehicle obstructions," *IEEE Trans. Intell. Transp. Syst.*, vol. 15, no. 5, pp. 2237–2248, Oct. 2014.

[30] R. He, O. Renaudin, V. M. Kolmonen, K. Haneda, Z. Zhong, B. Ai, S. Hubert, and C. Oestges, "Vehicle-to-vehicle radio channel characterization in crossroad scenarios," *IEEE Trans. Veh. Technol.*, vol. 65, no. 8, pp. 5850–5861, Aug. 2016.

[31] I. Sen and D. W. Matolak, "Vehicle-vehicle channel models for the 5-GHz band," *IEEE Trans. Intell. Transp. Syst.*, vol. 9, no. 2, pp. 235–245, Jun. 2008.

[32] O. Renaudin, V. M. Kolmonen, P. Vainikainen, and C. Oestges, "Car-to-car channel models based on wideband MIMO measurements at 5.3 GHz," in *Proc. EuCAP'09*, Berlin, Germany, Mar. 2009, pp. 635–639.

[33] L. Bernadó, T. Zemen, F. Tufvesson, A. F. Molisch, and C. F. Mecklenbrüker, "Delay and doppler spreads of nonstationary vehicular channels for safety-relevant scenarios," *IEEE Trans. Veh. Technol.*, vol. 63, no. 1, pp. 82–93, Jan. 2014.

[34] J. Kunisch and J. Pamp, "Wideband car-to-car radio channel measurements and model at 5.9 GHz," in *Proc. IEEE VTC'08*, Calgary, Canada, Sept. 2008, pp. 1–5.

[35] A. Paier, L. Bernado, J. Karedal, O. Klemp, and A. Kwoczek, "Overview of vehicle-to-vehicle radio channel measurements for collision avoidance applications," in *Proc. IEEE VTC-Spring'10*, Taipei, May 2010, pp. 1–5.

[36] L. Bernadó, T. Zemen, F. Tufvesson, A. F. Molisch, and C. F. Mecklenbräuker, "The (in-) validity of the WSSUS assumption in vehicular radio channels," in *Proc. IEEE PIMRC'12*, Sydney, Australian, Sept. 2012, pp. 1757–1762.

[37] M. Herdin, N. Czink, H. Ozcelik, and E. Bonek, "Correlation matrix distance, a meaningful measure for evaluation of non-stationary MIMO channels," in *Proc. IEEE VTC-Spring'05*, vol. 1, Stockholm, Sweden, May 2005, pp. 136–140.

[38] X. Ye, X. Cai, Y. Shen, X. Yin, and X. Cheng, "A geometry-based path loss model for high-speed-train environments in LTE-A networks," in *Proc. ICNC'2016*, Kauai, HI, Feb. 2016, pp. 1–6.

[39] R. He, A. F. Molisch, Z. Zhong, B. Ai, J. Ding, R. Chen, and Z. Li, "Measurement based channel modeling with directional antennas for high-speed railways," in *Proc. IEEE WCNC'13*, Shanghai, China, Apr. 2013, pp. 2932–2936.

[40] R. He, Z. Zhong, B. Ai, and J. Ding, "An empirical path loss model and fading analysis for high-speed railway viaduct scenarios," *IEEE Antennas Wireless Propag. Lett.*, vol. 10, pp. 808–812, 2011.

[41] ——, "Propagation measurements and analysis for high-speed railway cutting scenario," *Electron. Lett.*, vol. 47, no. 21, pp. 1167–1168, Oct. 2011.

[42] J. Lu, G. Zhu, and C. Briso-Rodriguez, "Fading characteristics in the railway terrain cuttings," in *Proc. IEEE VTC-Spring'11*, Yokohama, Japan, May 2011, pp. 1–5.

[43] R. He, Z. Zhong, B. Ai, and J. Ding, "Measurements and analysis of short-term fading behavior for high-speed rail viaduct scenario," in *Proc. IEEE ICC'12*, Ottawa, ON, Jun. 2012, pp. 4563–4567.

[44] R. He, Z. Zhong, B. Ai, J. Ding, Y. Yang, and A. F. Molisch, "Short-term fading behavior in high-speed railway cutting scenario: Measurements, analysis, and statistical models," *IEEE Trans Antennas Propag.*, vol. 61, no. 4, pp. 2209–2222, Apr. 2013.

[45] B. Chen, Z. Zhong, and B. Ai, "Stationarity intervals of time-variant channel in high speed railway scenario," *J. China Commun.*, vol. 9, no. 8, pp. 64–70, Aug. 2012.

[46] ——, "Non-stationary channel characteristics in high-speed railway," in *Proc. IEEE APS'15*, Vancouver, BC, Jul. 2015, pp. 97–98.

[47] F. Luan, Y. Zhang, L. Xiao, C. Zhou, and S. Zhou, "Fading characteristics of wireless channel on high-speed railway in hilly terrain scenario," *Int. J. Antennas Propag.*, vol. 2013, no. 3, pp. 188–192, 2013.

[48] P. Kyösti, et al., "WINNER II channel models," IST-4-027756, WINNER II D1.1.2, v1.2, Apr. 2008.

[49] L. Liu, C. Tao, J. Qiu, H. Chen, L. Yu, W. Dong, and Y. Yuan, "Position-based modeling for wireless channel on high-speed railway under a viaduct at 2.35 GHz," *IEEE J. Sel. Areas Commun.*, vol. 30, no. 4, pp. 834–845, May 2012.

[50] L. Tian and J. Zhang, "Analysis on non-stationary characteristics of wideband radio channel in HSR U-shape cutting scenario," in *Proc. IEEE ICCC'14*, Shanghai, China, Oct. 2014, pp. 544–548.

[51] T. S. Rappaport *et al.*, *Wireless communications: principles and practice*. Prentice Hall, New Jersey, 1996.

[52] M. Herdin, N. Czink, H. Ozcelik, and E. Bonek, "Correlation matrix distance, a meaningful measure for evaluation of non-stationary MIMO channels," in *Proc. IEEE VTC-Spring'05*, vol. 1, Stockholm, Sweden, May 2005, pp. 136–140.

[53] Y. Azar, G. N. Wong, K. Wang, R. Mayzus, J. K. Schulz, H. Zhao, F. Gutierrez, D. Hwang, and T. S. Rappaport, "28 GHz propagation measurements for outdoor cellular communications using steerable beam

[54] G. R. MacCartney, J. Zhang, S. Nie, and T. S. Rappaport, "Path loss models for 5G millimeter wave propagation channels in urban microcells," in *Proc. IEEE GLOBECOM'13*, Atlanta, GA, Dec. 2013, pp. 3948–3953.

[55] T. S. Rappaport, F. Gutierrez, E. Ben-Dor, J. N. Murdock, Y. Qiao, and J. I. Tamir, "Broadband millimeter-wave propagation measurements and models using adaptive-beam antennas for outdoor urban cellular communications," *IEEE Trans. Antennas Propag.*, vol. 61, no. 4, pp. 1850–1859, Apr. 2013.

[56] S. Sun, G. R. MacCartney, M. K. Samimi, S. Nie, and T. S. Rappaport, "Millimeter wave multi-beam antenna combining for 5G cellular link improvement in New York city," in *Proc. IEEE ICC'15*, Sydney, Australian, Jun. 2014, pp. 5468–5473.

[57] G. R. MacCartney and T. S. Rappaport, "73 GHz millimeter wave propagation measurements for outdoor urban mobile and backhaul communications in New York city," in *Proc. IEEE ICC'14*, Sydney, Australia, Jun. 2014, pp. 4862–4867.

[58] Q. Zhao and J. Li, "Rain attenuation in millimeter wave ranges," in *Proc. ISAPE'06*, Guilin, China, Oct. 2006, pp. 1–4.

[59] A. Kajiwara, "LMDS radio channel obstructed by foliage," in *Proc. IEEE ICC'00*, vol. 3, New Orleans, LA, Jun. 2000, pp. 1583–1587.

[60] X. Zhao, Q. Wang, S. Li, S. Geng, M. Wang, S. Sun, and Z. Wen, "Attenuation by human bodies at 26 and 39.5 GHz millimeter wave bands," *IEEE Antennas Wireless Propag. Lett.*, vol. 16, no. 99, pp. 1229–1232, 2016.

[61] H. Zhao, R. Mayzus, S. Sun, M. Samimi, J. K. Schulz, Y. Azar, K. Wang, G. N. Wong, F. Gutierrez, and T. S. Rappaport, "28 GHz millimeter wave cellular communication measurements for reflection and penetration loss in and around buildings in New York city," in *Proc. IEEE ICC'13*, Jun. 2013, pp. 5163–5167.

[62] K. Sato, T. Manabe, T. Ihara, H. Saito, S. Ito, T. Tanaka, K. Sugai, N. Ohmi, Y. Murakami, M. Shibayama, Y. Konishi, and T. Kimura, "Measurements of reflection and transmission characteristics of interior structures of office building in the 60 GHz band," *IEEE Trans. Antennas Propag.*, vol. 45, no. 12, pp. 1783–1792, Dec. 1997.

[63] S. Rajagopal, S. Abu-Surra, and M. Malmirchegini, "Channel feasibility for outdoor non-line-of-sight mmwave mobile communication," in *Proc. IEEE VTC'12-Fall*, Sep. 2012, pp. 1–6.

[64] A. Maltsev *et al.*, IEEE doc. 802.11ad 09/0334r8,2014, "Channel models for 60 GHz WLAN systems", May. 2009.

[65] A. Maltsev, R. Maslennikov, A. Sevastyanov, A. Khoryaev, and A. Lomayev, "Experimental investigations of 60 GHz WLAN systems in office environment," *IEEE J. Sel. Areas Commun.*, vol. 27, no. 8, pp. 1488–1499, Oct. 2009.

[66] M. Kyrö, V. Ranvier, V. M. Kolmonen, K. Haneda, and P. Vainikainen, "Long range wideband channel measurements at 81-86 GHz frequency range," in *Proc. EuCAP'10*, Barcelona, Spain, Apr. 2010, pp. 1–5.

[67] T. S. Rappaport, R. W. Heath, R. Daniels, and J. Murdock, *Millimeter Wave Wireless Communications*. Englewood Cliffs, NJ, USA: Peasron/Prentice-Hall, 2015.

[68] G. Lovnes, J. J. Reis, and R. H. Raekken, "Channel sounding measurements at 59 GHz in city streets," in *Proc. IEEE PIMRC'94*, vol. 2, Hague, Netherlands, Sept. 1994, pp. 496–500.

[69] S. Sun, T. S. Rappaport, R. W. Heath, A. Nix, and S. Rangan, "MIMO for millimeter-wave wireless communications: beamforming, spatial multiplexing, or both?" *IEEE Commun. Mag.*, vol. 52, no. 12, pp. 110–121, Dec. 2014.

[70] G. R. MacCartney, M. K. Samimi, and T. S. Rappaport, "Exploiting directionality for millimeter-wave wireless system improvement," in *Proc. IEEE ICC'15*, London, UK, Jun. 2015, pp. 2416–2422.

[71] M. K. Samimi and T. S. Rappaport, "3-D millimeter-wave statistical channel model for 5G wireless system design," *IEEE Trans. Microw. Theory Tech.*, vol. 64, no. 7, pp. 2207–2225, Jul. 2016.

[72] M. K. Samimi and T. S. Rappaport, "3-D statistical channel model for millimeter-wave outdoor mobile broadband communications," in *Proc. IEEE ICC'15*, London, UK, Jun. 2015, pp. 2430–2436.

[73] H2020-ICT-671650-mmMAGIC/D2.2, v1, "Measurement results and final mmMAGIC channel models," Dec. 2017.

[74] X. Wu, C.-X. Wang, J. Sun, J. Huang, R. Feng, Y. Yang, and X. Ge, "60-GHz millimeter-wave channel measurements and modeling for indoor office environments," *IEEE Trans. Antennas Propag.*, vol. 65, no. 4, pp. 1912–1924, Apr. 2017.

[75] S. Wu, C.-X. Wang, e. H. M. Aggoune, M. M. Alwakeel, and Y. He, "A non-stationary 3-D wideband twin-cluster model for 5G massive MIMO channels," *IEEE J. Sel. Areas Commun.*, vol. 32, no. 6, pp. 1207–1218, Jun. 2014.

This article has been accepted for publication in a future issue of this journal, but has not been fully edited. Content may change prior to final publication. Citation information: DOI 10.1109/COMST.2018.2862141, IEEE Communications Surveys & Tutorials

IEEE COMMUNICATIONS SURVEYS & TUTORIALS, VOL. XX, NO. XX, MONTH 2018   23

[76] S. Wu, C.-X. Wang, H. Haas, e. H. M. Aggoune, M. M. Alwakeel, and B. Ai, "A non-stationary wideband channel model for massive MIMO communication systems," *IEEE Trans. Wireless Commun.*, vol. 14, no. 3, pp. 1434–1446, Mar. 2015.

[77] H. Wu, S. Jin, and X. Gao, "Non-stationary multi-ring channel model for massive MIMO systems," in *Proc. WCSP'15*, Nanjing, China, Oct. 2015, pp. 1–6.

[78] Y. Chen, Y. Li, S. Sun, X. Cheng, and X. Chen, "A twin-multi-ring channel model for massive MIMO system," in *Proc. ISCIT'16*, Qingdao, China, Sept. 2016, pp. 606–610.

[79] C. F. Lopez, C.-X. Wang, and R. Feng, "A novel 2D non-stationary wideband massive MIMO channel model," in *Proc. IEEE CAMAD'16*, Toronto, Canada, Oct. 2016, pp. 207–212.

[80] C. F. Lopez and C.-X. Wang, "Novel 3D non-stationary wideband models for massive MIMO channels," *IEEE Trans. Wireless Commun.*, vol. 17, no. 5, pp. 2893-C2905, May 2018.

[81] A. O. Martinez, P. Eggers, and E. D. Carvalho, "Geometry-based stochastic channel models for 5G: extending key features for massive MIMO," in *Proc. IEEE PIMRC'16*, Valencia, Spain, Sept. 2016, pp. 1–6.

[82] X. Gao, J. Flordelis, G. Dahman, F. Tufvesson, and O. Edfors, "Massive MIMO channel modeling — extension of the COST 2100 model," in *Proc. JNCW'15*, Barcelona, Spain, Oct. 2015.

[83] X. Gao, F. Tufvesson, and O. Edfors, "Massive MIMO channels - measurements and models," in *Proc. ASILOMAR'13*, Pacific Grove, California, Nov. 2013, pp. 280–284.

[84] L. Liu, C. Oestges, J. Poutanen, K. Haneda, P. Vainikainen, F. Quitin, F. Tufvesson, and P. D. Doncker, "The COST 2100 MIMO channel model," *IEEE Wireless Commun. Mag.*, vol. 19, no. 6, pp. 92–99, Dec. 2012.

[85] Y. Xie, B. Li, X. Zuo, M. Yang, and Z. Yan, "A 3D geometry-based stochastic model for 5G massive MIMO channels," in *Proc. QSHINE'15*, Aug. 2015, pp. 216–222.

[86] S. Dahiya, "A statistical block fading channel model for multiuser massive MIMO system," in *Proc. SPCOM'16*, Bangalore, Jun. 2016, pp. 1–5.

[87] J. Joung, E. Kurniawan, and S. Sun, "Channel correlation modeling and its application to massive MIMO channel feedback reduction," *IEEE Trans. Veh. Technol.*, vol. 66, no. 5, pp. 3787–3797, 2016.

[88] S. Wu, C.-X. Wang, E. H. M. Aggoune, and M. M. Alwakeel, "A novel Kronecker-based stochastic model for massive MIMO channels," in *Proc. IEEE ICCC'15*, Shenzhen, China, Nov. 2015, pp. 1–6.

[89] Y. Yu, P. F. Cui, J. She, Y. Liu, X. Yang, W. J. Lu, S. Jin, and H. B. Zhu, "Measurement and empirical modeling of massive MIMO channel matrix in real indoor environment," in *Proc. WCSP'16*, Yangzhou, China, Oct. 2016, pp. 1–5.

[90] R. Zhang, Z. Zhong, J. Zhao, B. Li, and K. Wang, "Channel measurement and packet-level modeling for V2I spatial multiplexing uplinks using massive MIMO," *IEEE Trans. Veh. Technol.*, vol. 65, no. 10, pp. 7831–7843, Oct. 2016.

[91] M. Mbeutcha, W. Fan, J. Hcjsclbæck, and G. F. Pedersen, "Evaluation of massive MIMO systems using time-reversal beamforming technique," in *Proc. IEEE PIMRC'16*, Valencia, Spain, Sept. 2016, pp. 1–6.

[92] J. Weng, X. Tu, Z. Lai, S. Salous, and J. Zhang, "Indoor massive MIMO channel modelling using ray-launching simulation," *Int. J. Antennas Propag.*, pp. 1–13, May 2014.

[93] M. Pätzold, B. O. Hogstad, N. Youssef, and D. Kim, "A MIMO mobile-to-mobile channel model: part I - the reference model," in *Proc. IEEE PIMRC'05*, vol. 1, Berlin, Germany, Sept. 2005, pp. 573–578.

[94] M. Pätzold, B. O. Hogstad, and N. Youssef, "Modeling, analysis, and simulation of MIMO mobile-to-mobile fading channels," *IEEE Trans. Wireless Commun.*, vol. 7, no. 2, pp. 510–520, Feb. 2008.

[95] L. C. Wang, W. C. Liu, and Y. H. Cheng, "Statistical analysis of a mobile-to-mobile Rician fading channel model," *IEEE Trans. Veh. Technol.*, vol. 58, no. 1, pp. 32–38, Jan. 2009.

[96] A. G. Zajić and G. L. Stüber, "Space-time correlated mobile-to-mobile channels: modelling and simulation," *IEEE Trans. Veh. Technol.*, vol. 57, no. 2, pp. 715–726, Mar. 2008.

[97] S. Yoo, S. Yoo, J. Lee, and K. Kim, "Modeling and characteristics of mobile-to-mobile wideband MIMO channel based on the geometrical multi-radii two-rings with specified frequency selectivity," in *Proc. EUCAP'12*, Prague, Czekh, Mar. 2012, pp. 2030–2034.

[98] D. Shen, J. Chen, M. Zhang, Y. Cui, and K. Wu, "A channel model of the wideband MIMO mobile-to-mobile systems," in *Proc. ICMMT'10*, Chengdu, China, May 2010, pp. 1432–1435.

[99] X. Cheng, C.-X. Wang, D. I. Laurenson, S. Salous, and A. V. Vasilakos, "An adaptive geometry-based stochastic model for non-isotropic MIMO mobile-to-mobile channels," *IEEE Trans. Wireless Commun.*, vol. 8, no. 9, pp. 4824–4835, Sept. 2009.

[100] X. Cheng, Q. Yao, M. Wen, C.-X. Wang, L. Y. Song, and B. L. Jiao, "Wideband channel modeling and intercarrier interference cancellation for vehicle-to-vehicle communication systems," *IEEE J. Sel. Areas Commun.*, vol. 31, no. 9, pp. 434–448, Sept. 2013.

[101] X. Cheng, Q. Yao, C.-X. Wang, B. Ai, G. L. Stüber, D. Yuan, and B. L. Jiao, "An improved parameter computation method for a MIMO V2V Rayleigh fading channel simulator under non-isotropic scattering environments," *IEEE Commun. Lett.*, vol. 17, no. 2, pp. 265–268, Feb. 2013.

[102] X. Cheng, C.-X. Wang, B. Ai, and H. Aggoune, "Envelope level crossing rate and average fade duration of nonisotropic vehicle-to-vehicle ricean fading channels," *IEEE Trans. Intell. Transp. Syst.*, vol. 15, no. 1, pp. 62–72, Feb. 2014.

[103] X. Cheng, C.-X. Wang, H. Wang, X. Gao, X. H. You, D. Yuan, B. Ai, Q. Huo, L. Y. Song, and B. L. Jiao, "Cooperative MIMO channel modeling and multi-link spatial correlation properties," *IEEE J. Sel. Areas Commun.*, vol. 30, no. 2, pp. 388–396, Feb. 2012.

[104] A. Chelli and M. Pätzold, "A non-stationary MIMO vehicle-to-vehicle channel model derived from the geometrical street model," in *Proc. IEEE VTC'11-Fall*, San Francisco, CA, Sept. 2011, pp. 1–6.

[105] L. Cheng, D. D. Stancil, and F. Bai, "A roadside scattering model for the vehicle-to-vehicle communication channel," *IEEE J. Sel. Areas Commun.*, vol. 31, no. 9, pp. 449–459, Sept. 2013.

[106] W. Zhou, M. Pätzold, W. Chen, and Z. He, "An ergodic wideband MIMO channel simulator based on the geometrical T-junction scattering model for vehicle-to-vehicle communications," in *Proc. ICCE'10*, Nha Trang, Aug. 2010, pp. 323–328.

[107] Q. Fu and W. Zhou, "Statistical analysis of a MIMO vehicle-to-vehicle channel model based on the geometrical scattering environments," in *Proc. ICISCE'12*, Shenzhen, China, Dec. 2012, pp. 1–5.

[108] A. Chelli, R. Hamdi, and M. S. Alouini, "A vehicle-to-infrastructure channel model for blind corner scattering environments," in *Proc. IEEE VTC-Fall'13*, Las Vegas, NV, Sept. 2013, pp. 1–6.

[109] A. G. Zajić and G. L. Stüber, "Three-dimensional modeling, simulation, and capacity analysis of space–time correlated mobile-to-mobile channels," *IEEE Trans. Veh. Technol.*, vol. 57, no. 4, pp. 2042–2054, Jul. 2008.

[110] A. G. Zajić and G. L. Stüber, "Three-dimensional modeling and simulation of wideband MIMO mobile-to-mobile channels," *IEEE Trans. Wireless Commun.*, vol. 8, no. 3, pp. 1260–1275, Mar. 2009.

[111] A. G. Zajić and G. L. Stüber, "Statistical properties of wideband MIMO mobile-to-mobile channels (special paper)," in *Proc. IEEE WCNC'08*, Mar. 2008, pp. 763–768.

[112] A. G. Zajić, G. L. Stüber, T. G. Pratt, and S. T. Nguyen, "Wideband MIMO mobile-to-mobile channels: geometry-based statistical modeling with experimental verification," *IEEE Trans. Veh. Technol.*, vol. 58, no. 2, pp. 517–534, Feb. 2009.

[113] Y. Yuan, C.-X. Wang, X. Cheng, B. Ai, and D. I. Laurenson, "Novel 3D geometry-based stochastic models for non-isotropic MIMO vehicle-to-vehicle channels," *IEEE Trans. Wireless Commun.*, vol. 13, no. 1, pp. 298–309, Jan. 2014.

[114] Y. Yuan, C.-X. Wang, Y. He, M. M. Alwakeel, and e. H. M. Aggoune, "3D wideband non-stationary geometry-based stochastic models for non-isotropic MIMO vehicle-to-vehicle channels," *IEEE Trans. Wireless Commun.*, vol. 14, no. 12, pp. 6883–6895, Dec. 2015.

[115] A. Chelli and M. Pätzold, "The impact of fixed and moving scatterers on the statistics of MIMO vehicle-to-vehicle channels," in *Proc. IEEE VTC'09*, Barcelona, Spain, Apr. 2009, pp. 1–6.

[116] A. Zajić, "Modeling impact of moving scatterers on Doppler spectrum in wideband vehicle-to-vehicle channels," in *Proc. EuCAP'15*, Lisbon, Portugal, May 2015, pp. 1–5.

[117] S. Yoo and K. Kim, "An improved temporal correlation model for vehicle-to-vehicle channels with moving scatterers," in *Proc. URSI AP-RASC'16*, Seoul, Korea, Aug. 2016, pp. 1391–1392.

[118] A. Richter, J. Salmi, and V. Koivunen, "Distributed scattering in radio channels and its contribution to MIMO channel capacity," in *Proc. EuCAP'06*, Nice, France, Nov. 2006, pp. 1–7.

[119] N. Czink, F. Kaltenberger, Y. Zhou, L. Bernadó, T. Zemen, and X. Yin, "Low-complexity geometry-based modeling of diffuse scattering," in *Proc EuCAP'10*, Barcelona, Spain, Apr. 2010, pp. 1–4.

[120] J. Karedal, F. Tufvesson, N. Czink, A. Paier, C. Dumard, T. Zemen, C. F. Mecklenbrauker, and A. F. Molisch, "A geometry-based stochastic MIMO model for vehicle-to-vehicle communications," *IEEE Trans. Wireless Commun.*, vol. 8, no. 7, pp. 3646–3657, Jul. 2009.

[121] D. W. Matolak and Q. Wu, "Channel models for V2V communications: a comparison of different approaches," in *Proc. EUCAP'11*, Rome, Italy, Apr. 2011, pp. 2891–2895.

[122] J. D. Parsons, *The Mobile Radio Propagation Channel, 2nd Edition*, Wiley, 2000.

[123] G. Acosta and M. A. Ingram, "Model development for the wideband expressway vehicle-to-vehicle 2.4 GHz channel," in *Proc. IEEE WCNC'06.*, vol. 3, Las Vegas, NV, Apr. 2006, pp. 1283–1288.

[124] G. Acosta and M. A. Ingram, "A ber-based partitioned model for a 2.4 GHz vehicle-to-vehicle expressway channel," *Wireless Pers. Commun.*, vol. 37, no. 3, pp. 421–443, 2006.

[125] G. Acosta and M. A. Ingram, "Doubly selective vehicle-to-vehicle channel measurements and modeling at 5.9 GHz," *Proc. int. symp. wireless Pers. Multimedia Commun.*, San Diego, USA, Sept. 2006.

[126] G. Acosta and M. A. Ingram, "Six time- and frequency- selective empirical channel models for vehicular wireless LANs," *IEEE Veh. Technol. Mag.*, vol. 2, no. 4, pp. 4–11, Dec. 2007.

[127] B. Wang, I. Sen, and D. W. Matolak, "Performance evaluation of 802.16e in vehicle to vehicle channels," in *Proc. IEEE VTC'07*, Baltimore, MD, USA, Sept. 2007, pp. 1406–1410.

[128] I. Sen and D. W. Matolak, "Vehicle-vehicle channel models for the 5 GHz band," *IEEE Trans. Intell. Trans. Sys.*, vol. 9, no. 2, pp. 235–245, Jun. 2008.

[129] D. W. Matolak and Q. Wu, "Markov models for vehicle-to-vehicle channel multipath persistence processes," in *Proc. IEEE WAVE'08*, Dearborn, Mich, Dec. 2008, pp. 8–9.

[130] J. Maurer, T. M. Schafer, and W. Wiesbeck, "A realistic description of the environment for inter-vehicle wave propagation modelling," in *Proc. IEEE VTC'01-Fall*, vol. 3, Atlantic City, USA, Sept. 2001, pp. 1437–1441.

[131] J. Maurer, T. Fugen, T. Schafer, and W. Wiesbeck, "A new inter-vehicle communications (IVC) channel model," in *Proc. IEEE VTC'04-Fall*, Los Angeles, USA, Sept. 2004, pp. 9–13.

[132] J. Maurer, T. Fugen, and W. Wiesbeck, "Physical layer simulations of IEEE802.11a for vehicle-to-vehicle communications," in *Proc. IEEE VTC'05-Fall*, vol. 3, Dallas, TX, USA, Sept. 2005, pp. 1849–1853.

[133] W. Wiesbeck and S. Knorzer, "Characteristics of the mobile channel for high velocities," in *Proc. ICEAA'07*, Torino, Italy, Sept. 2007, pp. 116–120.

[134] L. Reichardt, T. Fugen, and T. Zwick, "Influence of antennas placement on car to car communications channel," in *Proc. EuCAP'09*, Berlin, Germany, Mar. 2009, pp. 630–634.

[135] J. Nuckelt, T. Abbas, F. Tufvesson, C. Mecklenbrauker, L. Bernado, and T. Kurner, "Comparison of ray tracing and channel-sounder measurements for vehicular communications," in *Proc. IEEE VTC'13-Spring*, Dresden, Germany, Jun. 2013, pp. 1–5.

[136] T. Abbas, J. Nuckelt, T. Krner, T. Zemen, C. F. Mecklenbräuker, and F. Tufvesson, "Simulation and measurement-based vehicle-to-vehicle channel characterization: accuracy and constraint analysis," *IEEE Trans. Antennas Propag.*, vol. 63, no. 7, pp. 3208–3218, Jul. 2015.

[137] B. Ai, K. Guan, M. Rupp, T. Kurner, X. Cheng, X. F. Yin, Q. Wang, G. Y. Ma, Y. Li, L. Xiong, and J. W. Ding, "Future railway services-oriented mobile communications network," *IEEE Commun. Mag.*, vol. 53, no. 10, pp. 78–85, Oct. 2015.

[138] D. T. Fokum and V. S. Frost, "A survey on methods for broadband internet access on trains," *IEEE Commun. Surveys Tuts.*, vol. 12, no. 2, pp. 171–185, Apr. 2010.

[139] F. Abrishamkar and J. Irvine, "Comparison of current solutions for the provision of voice services to passengers on high speed trains," in *Proc. IEEE VTC'00-Fall*, Boston, MA, USA, Sept. 2000, pp. 1498–1505.

[140] B. Ai, R. He, Z. Zhong, K. Guan, B. Chen, P. Liu, and Y. Li, "Radio wave propagation scene partitioning for high-speed rails," *Int. J. Antennas Propag.*, vol. 2012, pp. 1072–1075, 2012.

[141] B. Chen and Z. Zhong, "Geometry-based stochastic modeling for MIMO channel in high-speed mobile scenario," *Int. J. Antennas Propag.*, vol. 2012, no. 2012, pp. 1174–1177, 2012.

[142] A. Ghazal, C.-X. Wang, B. Ai, D. Yuan, and H. Haas, "A nonstationary wideband MIMO channel model for high-mobility intelligent transportation systems," *IEEE Trans. Intell. Transp. Syst.*, vol. 16, no. 2, pp. 885–897, Apr. 2015.

[143] A. Ghazal, C.-X. Wang, Y. Liu, P. Fan, and M. K. Chahine, "A generic non-stationary MIMO channel model for different high-speed train scenarios," in *Proc. IEEE ICCC'15*, Shenzhen, China, Nov. 2015, pp. 1–6.

[144] T. Zhou, C. Tao, L. Liu, and Z. Tan, "A semi-empirical MIMO channel model for high-speed railway viaduct scenarios," in *Proc. IEEE ICC'14*, Sydney, NSW, Australia, Jun. 2014, pp. 5854–5858.

[145] B. Chen, Z. Zhong, B. Ai, and D. G. Michelson, "A geometry-based stochastic channel model for high-speed railway cutting scenarios," *IEEE Antennas Wireless Propag. Lett.*, vol. 14, pp. 851–854, 2015.

[146] Y. Liu, C.-X. Wang, C. F. Lopez, and X. Ge, "3D non-stationary wideband circular tunnel channel models for high-speed train wireless communication systems," *Sci. China Inf. Sci.*, vol. 60, no. 8, Aug. 2017.

[147] X. Yin, X. Cai, X. Cheng, J. Chen, and M. Tian, "Empirical geometry-based random-cluster model for high-speed-train channels in UMTS networks," *IEEE Trans. Intell. Transp. Syst.*, vol. 16, no. 5, pp. 2850–2861, Oct. 2015.

[148] ITU-R M.2135-1, "Guidelines for evaluation of radio interface technologies for IMT-Advanced," Gneva, Switzerland, Rep. ITU-R M.2135-1, Dec. 2009.

[149] A. Ghazal, Y. Yuan, C.-X. Wang, Y. Zhang, Q. Yao, H. Zhou, and W. Duan, "A non-stationary IMT-Advanced MIMO channel model for high-mobility wireless communication systems," *IEEE Trans. Wireless Commun.*, vol. 16, no. 4, pp. 2057–2068, Apr. 2017.

[150] J. Bian, J. Sun, C.-X. Wang, R. Feng, J. Huang, Y. Yang, and M. Zhang, "A WINNER+ based 3-D non-stationary wideband MIMO channel model," *IEEE Trans. Wireless Commun.*, vol. 17, no. 3, pp. 1755–1767, Mar. 2018.

[151] R. He, B. Ai, Z. Zhong, A. F. Molisch, R. Chen, and Y. Yang, "A measurement-based stochastic model for high-speed railway channels," *IEEE Trans. Intell. Transp. Syst.*, vol. 16, no. 3, pp. 1120–1135, Jun. 2015.

[152] S. Lin, Z. Zhong, L. Cai, and Y. Luo, "Finite state markov modelling for high speed railway wireless communication channel," in *Proc. IEEE GLOBECOM'12*, Anaheim, CA, America, Dec. 2012, pp. 5421–5426.

[153] X. Li, C. Shen, B. Ai, and G. Zhu, "Finite-state markov modeling of fading channels: a field measurement in high-speed railways," in *Proc. IEEE ICCC'13*, Xi'an, China, Aug. 2013, pp. 577–582.

[154] L. Liu, C. Tao, J. Qiu, H. Chen, L. Yu, W. Dong, and Y. Yuan, "Position-based modeling for wireless channel on high-speed railway under a viaduct at 2.35 GHz," *IEEE J. Sel. Areas Commun.*, vol. 30, no. 4, pp. 834–845, May 2012.

[155] L. Liu, C. Tao, J. Qiu, T. Zhou, R. Sun, and H. Chen, "The dynamic evolution of multipath components in high-speed railway in viaduct scenarios: from the birth-death process point of view," in *Proc. IEEE PIMRC'12*, Sydney, Australian, Sep. 2012, pp. 1774–1778.

[156] L. Liu, C. Tao, R. Sun, H. Chen, and Z. Lin, "Non-stationary channel characterization for high-speed railway under viaduct scenarios," *Sci. Bulletin*, vol. 59, no. 35, pp. 4988–4998, 2014.

[157] T. Pedersen and B. H. Fleury, "Radio channel modelling using stochastic propagation graphs," in *Proc. IEEE ICC'07*, Glasgow, UK, Jun. 2007, pp. 2733–2738.

[158] L. Tian, X. Yin, Q. Zuo, J. Zhou, Z. Zhong, and S. X. Lu, "Channel modeling based on random propagation graphs for high speed railway scenarios," in *Proc. IEEE PIMRC'12*, Sydney, Australian, Sept. 2012, pp. 1746–1750.

[159] S. Knörzer, M. A. Baldauf, T. Fugen, and W. Wiesbeck, "Channel analysis for an OFDM-MISO train communications system using different antennas," in *Proc. IEEE VTC'07*, Baltimore, MD, Sept. 2007, pp. 809–813.

[160] K. Guan, Z. Zhong, B. Ai, and T. Kürner, "Deterministic propagation modeling for the realistic high-speed railway environment," in *Proc. IEEE VTC'13-Spring*, Dresden, Germany, Jun. 2013, pp. 1–5.

[161] J. Yang, B. Ai, K. Guan, D. He, R. He, B. Zhang, Z. Zhong, Z. Zhao, D. Miao, and H. Guan, "Deterministic modeling and stochastic analysis for channel in composite high-speed railway scenario," in *Proc. IEEE VTC'16-Spring*, Nanjing, China, May 2016, pp. 1–5.

[162] Y. Liu, C.-X. Wang, A. Ghazal, S. Wu, and W. Zhang, "A multi-mode waveguide tunnel channel model for high-speed train wireless communication systems," in *Proc. EuCAP'15*, Lisbon, Portugal, May 2015, pp. 1–5.

[163] M. K. Samimi and T. S. Rappaport, "Statistical channel model with multi-frequency and arbitrary antenna beamwidth for millimeter-wave outdoor communications," in *Proc. IEEE GC Wkshps'15*, San Diego, CA, Dec. 2015, pp. 1–7.

[164] M. Samimi, K. Wang, Y. Azar, G. N. Wong, R. Mayzus, H. Zhao, J. K. Schulz, S. Sun, F. Gutierrez, and T. S. Rappaport, "28 GHz angle of arrival and angle of departure analysis for outdoor cellular communications using steerable beam antennas in New York city," in *Proc. IEEE VTC'13-Spring*, Dresden, Germany, Jun. 2013, pp. 1–6.

[165] S. Deng, C. J. Slezak, G. R. MacCartney, and T. S. Rappaport, "Small wavelengths — big potential: millimeter wave propagation measurements for 5G," *Microw. J.*, vol. 57, no. 11, pp. 4–12, 2014.

[166] G. R. MacCartney, M. K. Samimi, and T. S. Rappaport, "Omnidirectional path loss models in new york city at 28 GHz and 73 GHz," in *Porc. IEEE PIMRC'14*, Washington, DC, USA, Sept. 2014, pp. 227–231.

[167] M. K. Samimi and T. S. Rappaport, "Ultra-wideband statistical channel model for non line of sight millimeter-wave urban channels," in *Proc. IEEE GLOBECOM'14*, Austin, TX, USA, Dec. 2014, pp. 3483–3489.

[168] T. S. Rappaport and S. Deng, "73 GHz wideband millimeter-wave foliage and ground reflection measurements and models," in *Proc. IEEE ICC'15*, London, UK, Jun. 2015, pp. 1238–1243.

[169] G. R. Maccartney, T. S. Rappaport, S. Sun, and S. Deng, "Indoor office wideband millimeter-wave propagation measurements and channel models at 28 and 73 GHz for ultra-dense 5G wireless networks," *IEEE Access*, vol. 3, pp. 2388–2424, 2015.

[170] S. Hur, S. Baek, B. Kim, Y. Chang, A. F. Molisch, T. S. Rappaport, K. Haneda, and J. Park, "Proposal on millimeter-wave channel modeling for 5G cellular system," *IEEE J. Sel. Topics Signal Process.*, vol. 10, no. 3, pp. 454–469, Apr. 2016.

[171] X. Zhao, S. Li, Q. Wang, M. Wang, S. Sun, and W. Hong, "Channel measurements, modeling, simulation and validation at 32 GHz in outdoor microcells for 5G radio systems," *IEEE Access*, vol. 5, pp. 1062–1072, Jan. 2017.

[172] 3GPP TR 38.900, V14.0.0, "Study on channel model for frequency spectrum above 6 GHz (Release 14)," Jun. 2016.

[173] Aalto University *et al.*, "5G channel model for bands up to 100 GHz," v2.0, Mar. 2014.

[174] A. A. M. Saleh and R. Valenzuela, "A statistical model for indoor multipath propagation," *IEEE J. Sel. Areas Commun.*, vol. 5, no. 2, pp. 128–137, Feb. 1987.

[175] Q. H. Spencer, B. D. Jeffs, M. A. Jensen, and A. L. Swindlehurst, "Modeling the statistical time and angle of arrival characteristics of an indoor multipath channel," *IEEE J. Sel. Areas Commun.*, vol. 18, no. 3, pp. 347–360, Mar. 2000.

[176] S.-K. Yong *et al.*, IEEE Tech. Rep. 15-07-0584-01-003c, "TG3c Channel Modeling Sub-Commitee Final Report," 2007.

[177] Y. Shoji, H. Sawada, C. S. Choi, and H. Ogawa, "A modified SV-model suitable for line-of-sight desktop usage of millimeter-wave WPAN systems," *IEEE Trans. Antennas Propag.*, vol. 57, no. 10, pp. 2940–2948, Oct. 2009.

[178] A. Maltsev, R. Maslennikov, A. Sevastyanov, A. Lomayev, and A. Khoryaev, "Statistical channel model for 60 GHz WLAN systems in conference room environment," in *Proc. EuCAP'10*, Apr. 2010, pp. 1–5.

[179] A. Maltsev *et al.*, IEEE doc. 802.11-08/1044r0, "60 GHz WLAN Experimental Investigations," Sept. 8, 2008.

[180] C. Gustafson, K. Haneda, S. Wyne, and F. Tufvesson, "On mm-wave multipath clustering and channel modeling," *IEEE Trans. Antennas Propag.*, vol. 62, no. 3, pp. 1445–1455, Mar. 2014.

[181] K. Haneda, J. Järveläinen, A. Karttunen, M. Kyrö, and J. Putkonen, "A statistical spatio-temporal radio channel model for large indoor environments at 60 and 70 GHz," *IEEE Trans. Antennas Propag.*, vol. 63, no. 6, pp. 2694–2704, Jun. 2015.

[182] J. Hubner, S. Zeisberg, K. Koora, J. Borowski, and A. Finger, "Simple channel model for 60 GHz indoor wireless LAN design based on complex wideband measurements," in *Proc. IEEE VTC'97*, vol. 2, Phoenix, AZ, USA, May 1997, pp. 1004–1008.

[183] P. Soma, L. C. Ong, S. Sun, and M. Y. W. Chia, "Propagation measurements and modeling of LMDS radio channel in singapore," *IEEE Trans. Veh. Technol.*, vol. 52, no. 3, pp. 595–606, May 2003.

[184] H. C. Nguyen, G. R. MacCartney, T. Thomas, T. S. Rappaport, B. Vejlgaard, and P. Mogensen, "Evaluation of empirical ray-tracing model for an urban outdoor scenario at 73 GHz E-band," in *Proc. IEEE VTC'14-Fall*, Vancouver, BC, Sept. 2014, pp. 1–6.

[185] S. Hur, S. Baek, B. Kim, J. Park, A. F. Molisch, K. Haneda, and M. Peter, "28 GHz channel modeling using 3D ray-tracing in urban environments," in *Proc. EuCAP'15*, Lisbon, Portugal, May 2015, pp. 1–5.

[186] A. Schiavoni, A. Leoni, D. Arena, and R. Lanzo, "Ray tracing simulations at millimeter waves in different indoor and outdoor scenarios," in *Proc. EuCAP'16*, Davos, Switzerland, Apr. 2016, pp. 1–5.

[187] S. Loredo, A. Rodriguez-Alonso, and R. P. Torres, "Indoor MIMO channel modeling by rigorous GO/UTD-based ray tracing," *IEEE Trans. Veh. Technol.*, vol. 57, no. 2, pp. 680–692, Mar. 2008.

[188] M. J. Kazemi, A. Abdipur, and A. Mohammadi, "Indoor propagation MIMO channel modeling in 60 GHz using SBR based 3D ray tracing technique," in *Proc. MMWaTT'12*, Tehran, Dec 2012, pp. 25–28.

[189] D. Murugesan and T. R. Rao, "Indoor corridor radio propagation characteristics at 60 GHz for wireless communications," in *Proc. IC-CCNT'2012*, Coimbatore, India, Jul. 2012, pp. 1–5.

[190] R. Felbecker, W. Keusgen, and M. Peter, "Ray-tracing simulations of the 60 GHz incabin radio channel," in *Proc. URSI'08*, Chicago, USA, 2008, pp. 1–4.

[191] Y. Chang, M. Furukawa, H. Suzuki, and K. Fukawa, "Propagation analysis with ray tracing method for high speed trains environment at 60 GHz," in *Proc. IEEE VTC'15-Spring*, Glasgow, UK, May 2015, pp. 1–5.

[192] Z. Hengkai, Z. Guoxin, Z. Li, F. Weiwei, W. Hui, and S. Hu, "Ray tracing analysis of Gaussian beamed millimetre wave propagation in circle tunnel," in *Proc. IET CCWMC'09*, Shanghai, China, Dec. 2009, pp. 164–167.

[193] J. Järveläinen, M. Kurkela, A. Karttunen, K. Haneda, and J. Putkonen, "70 GHz radio wave propagation prediction in a large office," in *Proc. LAPC'14*, Loughborough, UK, Nov. 2014, pp. 420–424.

[194] J. Järveläinen and K. Haneda, "Sixty gigahertz indoor radio wave propagation prediction method based on full scattering model," *Radio Sci.*, vol. 49, no. 4, pp. 293–305, Apr. 2014.

[195] J. Järveläinen, K. Haneda, and A. Karttunen, "Indoor propagation channel simulations at 60 GHz using point cloud data," *IEEE Trans. Antennas Propag.*, vol. 64, no. 10, pp. 4457–4467, Oct. 2016.

[196] L. Tian, V. Degli-Esposti, E. M. Vitucci, and X. Yin, "Semi-deterministic radio channel modeling based on graph theory and ray-tracing," *IEEE Trans. Antennas Propag.*, vol. 64, no. 6, pp. 2475–2486, Jun. 2016.

[197] V. Degli-Esposti, F. Fuschini, E. M. Vitucci, and G. Falciasecca, "Measurement and modelling of scattering from buildings," *IEEE Trans. Antennas Propag.*, vol. 55, no. 1, pp. 143–153, Jan. 2007.

[198] J. Chen, X. Yin, L. Tian, and M. D. Kim, "Millimeter-wave channel modeling based on a unified propagation graph theory," *IEEE Commun. Lett.*, vol. 21, no. 2, pp. 246–249, Feb. 2017.

[199] R. Verdone and A. Zanella, *Pervasive Mobile and Ambient Wireless Communications*. London: Springer, 2012.

[200] A. Maltsev, A. Pudeyev, I. Karls, I. Bolotin, G. Morozov, R. Weiler, M. Peter, and W. Keusgen, "Quasi-deterministic approach to mmwave channel modeling in a non-stationary environment," in *Proc. IEEE GC Wkshps'14*, Austin, TX, USA, 2014, pp. 966–971.

[201] S. Jaeckel, L. Raschkowski, K. Börner, and L. Thiele, "QuaDRiGa: A 3-D multi-cell channel model with time evolution for enabling virtual field trials," *IEEE Trans. Antennas Propag.*, vol. 62, no. 6, pp. 3242–3256, Jun. 2014.

[202] S. Jaeckel, L. Raschkowski, K. Börner, L. Thiele, F. Burkhardt, and E. Eberlein, "QuaDRiGa-Quasi Deterministic Radio Channel Generator, user manual and documentation," Fraunhofer Heinrich Hertz institute, Tech. Rep. v2.0.0, Aug. 2017.

[203] 3GPP TR 38.901, V14.0.0, "Study on channel model for frequencies from 0.5 to 100 GHz (Release 14)," Mar. 2017.

[204] ITU-R, "Preliminary draft new report ITU-R M. [IMT-2020.EVAL]," Niagara Falls, Canada, R15-WP5D-170613-TD-0332, Jun. 2017.

[205] A. Maltsev *et al.*, IEEE doc. 802.11-15/1150r9, "Channel models for IEEE 802.11ay," 2016.

[206] S. Wu, C. X. Wang, M. Aggoune, M. M. Alwakeel, and X. H. You, "A general 3D non-stationary 5G wireless channel model," *IEEE Trans. Commun.*, vol. 66, no. 7, pp. 3065–3078, July 2018.

[207] ITU-R, Recommendation P.1816-3, "The prediction of the time and the spatial profile for broadband land mobile services using UHF and SHF bands," Jul., 2015.

[208] L. M. Correia, *Wireless Flexible Personalised Communications: COST 259: European Cooperation in Mobile Radio Research*. John Wiley & Sons, 1997.

[209] N. Czink and C. Oestges, "The COST 273 MIMO channel model: three kinds of clusters," in *Proc. IEEE ISSSTA'08*, Bologna, Italy, Aug. 2008, pp. 282–286.

[210] E. Ben-Dor, T. S. Rappaport, Y. Qiao, and S. J. Lauffenburger, "Millimeter-wave 60 Ghz outdoor and vehicle AOA propagation measurements using a broadband channel sounder," in *Proc GLOBECOM'11*, Houston, Texas, USA, Dec. 2011, pp. 1–6.

[211] K. Bakowski and K. Wesolowski, "Change the channel," *IEEE Veh. Technol. Mag.*, vol. 6, no. 2, pp. 82–91, Jun. 2011.

[212] 3GPP TR 36.873, V12.0.0, "3rd Generation Partnership Project, Technical Specification Group Radio Access Network, Study on 3D channel model for LTE (Release 12)," Jun. 2015.

[213] T. Jämsä and P. Kyösti, "Device-to-device extension to geometry-based stochastic channel models," in *Proc. EuCAP'15, Lisbon, Portugal*, May 2015, pp. 1–4.

[214] Z. Wang, E. K. Tameh, and A. R. Nix, "A sum-of-sinusoids based simulation model for the joint shadowing process in urban peer-to-peer

[215] radio channels," in *Proc. IEEE VTC'05-Fall, Dallas, TX, USA*, vol. 3, Sept. 2005, pp. 1732–1736.

[215] V. Nurmela *et al.*, METIS, ICT-317669/D1.2, "Initial channel models based on measurements," Apr. 2014.

[216] 3GPP TR 25.996 v12.0.0, "Spatial channel model for multiple input multiple output (MIMO) simulations," Release 12, Sept. 2014.

[217] Y. Wang, L. Huang, Z. Shi, K. Liu, and X. Zou, "A millimeter wave channel model with variant angles under 3GPP SCM framework," in *Proc. IEEE PIMRC'15 Workshop*, Hong Kong, China, Aug. 2015, pp. 2249–2254.

[218] N. Iqbal, J. Luo, C. Schneider, D. Dupleich, S. Haefner, R. Mller, and R. S. Thoma, "Frequency and bandwidth dependence of millimeter wave ultra-wide-band channels," in *Proc. EUCAP'17*, Paris, France, Mar. 2017, pp. 141–145.

[219] Q. Zhu, H. Li, Y. Fu, C.-X. Wang, Y. Tan, X. Chen, and Q. Wu, "A novel 3D non-stationary wireless MIMO channel simulator and hardware emulator," *IEEE Trans. Commun.*, accepted for publication.

[220] H. J. Song and T. Nagatsuma, "Present and future of terahertz communications," *IEEE Trans. THz Sci. Technol.*, vol. 1, no. 1, pp. 256–263, Sept. 2011.

[221] T. Küner, "Towards tuture THz communications systems," *THz. Sci. Technol.*, vol. 5, no. 1, pp. 11–17, 2012.

[222] ITU-R Rec. P.676-8, "Attenuation by atmospheric gases," 2009.

[223] Y. Choi, J. W. Choi, and J. M. Cioffi, "A geometric-statistic channel model for THz indoor communications," *J. Infrared Milli. THz. Waves*, vol. 34, no. 7, pp. 456–467, 2013.

[224] C. Han, A. O. Bicen, and I. F. Akyildiz, "Multi-ray channel modeling and wideband characterization for wireless communications in the terahertz band," *IEEE Trans. Wireless Commun.*, vol. 14, no. 5, pp. 2402–2412, May 2015.

[225] P. H. Pathak, X. Feng, P. Hu, and P. Mohapatra, "Visible light communication, networking, and sensing: a survey, potential and challenges," *IEEE Commun. Survey Tuts*, vol. 17, no. 4, pp. 2047–2077, Fourthquarter 2015.

[226] Y. A. Alqudah and M. Kavehrad, "MIMO characterization of indoor wireless optical link using a diffuse-transmission configuration," *IEEE Trans. Commun.*, vol. 51, no. 9, pp. 1554–1560, Sept. 2003.

[227] F. Miramirkhani, O. Narmanlioglu, M. Uysal, and E. Panayirci, "A mobile channel model for VLC and application to adaptive system design," *IEEE Commun. Lett.*, vol. 21, no. 5, pp. 1035–1038, May 2017.

[228] F. Miramirkhani and M. Uysal, "Channel modeling and characterization for visible light communications," *IEEE Photon. J.*, vol. 7, no. 6, pp. 1–16, Dec. 2015.

[229] A. Al-Kinani, C.-X. Wang, H. Haas, and Y. Yang, "Characterization and modeling of visible light communication channels," in *Proc. VTC'16-Spring*, Nanjing, China, May 2016, pp. 1–5.

[230] ——, "A geometry-based multiple bounce model for visible light communication channels," in *Proc. IWCMC'16*, Paphos, Cyprus, Sept. 2016, pp. 31–37.

[231] J. Wang, A. Al-Kinani, W. Zhang, C.-X. Wang, and L. Zhou, "A general channel model for visible light communications in underground mines," *China Commun.*, vol. 15, no. 10, Oct. 2018.

[232] Al-Kinani, C.-X. Wang, L. Zhou, and W. Zhang, "Channel measurements and models for optical wireless communications: A survey," *IEEE Commun. Surveys Tuts.*, vol. 20, no. 3, 3rd Quart., 2018.

[233] T. Nakano and J. Q. Liu, "Design and analysis of molecular relay channels: An information theoretic approach," *IEEE Trans. Nanobiosci.*, vol. 9, no. 3, pp. 213–221, Sept. 2010.

[234] T. Nakano, Y. Okaie, and J. Q. Liu, "Channel model and capacity analysis of molecular communication with brownian motion," *IEEE Commun. Lett.*, vol. 16, no. 6, pp. 797–800, Jun. 2012.

[235] A. O. Bicen, I. F. Akyildiz, S. Balasubramaniam, and Y. Koucheryavy, "Linear channel modeling and error analysis for intra/inter-cellular Ca2+ molecular communication," *IEEE Trans. Nanobiosci.*, vol. 15, no. 5, pp. 488–498, Jul. 2016.

[236] N. Garralda, I. Llatser, A. Cabellos-Aparicio, and M. Pierobon, "Simulation-based evaluation of the diffusion-based physical channel in molecular nanonetworks," in *IEEE INFOCOM WKSHPS'11*, Shanghai, China, Apr. 2011, pp. 443–448.

[237] A. Emslie, R. Lagace, and P. Strong, "Theory of the propagation of UHF radio waves in coal mine tunnels," *IEEE Trans. Antennas Propag.*, vol. 23, no. 2, pp. 192–205, Mar. 1975.

[238] G. Poitau and A. Kouki, "Analysis of MIMO capacity in waveguide environments using practical antenna structures for selective mode excitation," in *Proc. CCGEI04*, vol. 1, Niagara, North America, May 2004, pp. 349–352.

[239] H. Wang, F. R. Yu, L. Zhu, T. Tang, and B. Ning, "Finite-state Markov modeling for wireless channels in tunnel communication-based train control systems," *IEEE Trans. Intell. Transp. Syst.*, vol. 15, no. 3, pp. 1083–1090, Jun. 2014.

[240] D. W. Matolak, "Channel characterization for unmanned aircraft systems," in *Proc. EuCAP'15*, Lisbon, Portugal, May 2015, pp. 1–5.

[241] D. W. Matolak and R. Sun, "Air-ground channel characterization for unmanned aircraft systems: The near-urban environment," in *Proc. IEEE MILCOM'15*, Tampa, FL, USA, Oct. 2015, pp. 1656–1660.

[242] ——, "Air-ground channel characterization for unmanned aircraft systems: The hilly suburban environment," in *Proc. IEEE VTC'14-Fall*, Vancouver, BC, Canada, Sept. 2014, pp. 1–5.

[243] R. Sun and D. W. Matolak, "Air-ground channel characterization for unmanned aircraft systems: The mountainous environment," in *Proc. IEEE/AIAA DASC'14*, Prague, Czech Republic, Sept. 2015, pp. 5C2–1–5C2–9.

[244] D. W. Matolak and R. Sun, "Air-ground channel characterization for unmanned aircraft systems: The over-freshwater setting," in *Proc. ICNS'14*, Apr. 2014, pp. K1–1–K1–9.

[245] K. Daniel, M. Putzke, B. Dusza, and C. Wietfeld, "Three dimensional channel characterization for low altitude aerial vehicles," in *Proc. ISWC-S'10*, York, UK, Sept. 2010, pp. 756–760.

[246] Z. Shi, P., Z. L. Huang, and C. Chen, "Modeling of wireless channel between uav and vessel using the FDTD method," in *Proc. WiCOM'14*, Beijing, China, Sept. 2014, pp. 100–104.

[247] D. W. Matolak, "Air-ground channels amp; models: Comprehensive review and considerations for unmanned aircraft systems," in *Proc. 2012 IEEE Aeros. Conf.*, Big Sky, MT, USA, Mar. 2012, pp. 1–17.

[248] D. W. Matolak and R. Sun, "Unmanned aircraft systems: Air-ground channel characterization for future applications," *IEEE Veh. Technol. Mag.*, vol. 10, no. 2, pp. 79–85, June 2015.

[249] L. Zeng, X. Cheng, C.-X. Wang, and X. Yin, "A 3D geometry-based stochastic channel model for UAV-MIMO channels," in *Proc. IEEE WCNC'17*, Mar. 2017, pp. 1–5.

[250] K. Jin, X. Cheng, X. Ge, and X. Yin, "Three dimensional modeling and space-time correlation for UAV channels," in *Proc. IEEE VTC'17-Spring*, Sydney, NSW, Australia, Jun. 2017, pp. 1–5.

[251] Y. Rissafi, L. Talbi, and M. Ghaddar, "Experimental characterization of an uwb propagation channel in underground mines," *IEEE Trans. Antennas Propag.*, vol. 60, no. 1, pp. 240–246, Jan. 2012.

[252] A. Salam, M. C. Vuran, and S. Irmak, "Pulses in the sand: Impulse response analysis of wireless underground channel," in *Proc. IEEE INFOCOM'16*, San Francisco, CA, USA, Apr. 2016, pp. 1–9.

[253] R. Feng, Y. Liu, J. Huang, J. Sun, C.-X. Wang, and G. Goussetis, "Channel parameter estimation algorithms: recent advances and future challenges," *China Commun.*, vol. 15, no. 5, pp. 211–228, May 2018.

[254] R. Feng, J. Huang, J. Sun, and C.-X. Wang, "A novel 3D frequency domain SAGE algorithm with applications to parameter estimation in mmwave massive MIMO indoor channels," *Sci. China Inf. Sci.*, vol. 60, no. 8, doi: 10.1007/s11432-017-9139-4, Aug. 2017.

[255] J. Zhang, "The interdisciplinary research of big data and wireless channel: a cluster-nuclei based channel model," *China Commun.*, vol. 13, no. Supplement2, pp. 14–26, 2016.

Cheng-Xiang Wang (S'01-M'05-SM'08-F'17) received the BSc and MEng degrees in Communication and Information Systems from Shandong University, China, in 1997 and 2000, respectively, and the PhD degree in Wireless Communications from Aalborg University, Denmark, in 2004.

He was a Research Assistant with the Hamburg University of Technology, Hamburg, Germany, from 2000 to 2001, a Visiting Researcher with Siemens AG Mobile Phones, Munich, Germany, in 2004, and a Research Fellow with the University of Agder, Grimstad, Norway, from 2001 to 2005. He has been with Heriot-Watt University, Edinburgh, U.K., since 2005, where he was promoted to a Professor in 2011. In 2018, he joined Southeast University, Nanjing, China, as a Professor and Thousand Talent Plan Expert. He has authored 2 books, one book chapter, and over 330 papers in refereed journals and conference proceedings. His current research interests include wireless channel modeling and (B)5G wireless communication networks, including green communications, cognitive radio networks, high mobility communication networks, massive MIMO, millimetre wave communications, and visible light communications.

Dr. Wang is a Fellow of the IET and HEA, and is recognized as a Web of Science 2017 Highly Cited Researcher. He served or is currently serving as an Editor for nine international journals, including the IEEE TRANSACTIONS ON VEHICULAR TECHNOLOGY since 2011, the IEEE TRANSACTIONS ON COMMUNICATIONS since 2015, and the IEEE TRANSACTIONS ON WIRELESS COMMUNICATIONS from 2007 to 2009. He was the leading Guest Editor of the IEEE JOURNAL ON SELECTED AREAS IN COMMUNICATIONS, Special Issue on Vehicular Communications and Networks. He is also a Guest Editor of the IEEE JOURNAL ON SELECTED AREAS IN COMMUNICATIONS, Special Issue on Spectrum and Energy Efficient Design of Wireless Communication Networks, and the IEEE TRANSACTIONS ON BIG DATA, Special Issue on Wireless Big Data. He served or is serving as a TPC Member, TPC Chair, and General Chair of over 80 international conferences. He received nine Best Paper Awards from the IEEE Globecom 2010, the IEEE ICCT 2011, ITST 2012, the IEEE VTC 2013, IWCMC 2015, IWCMC 2016, the IEEE/CIC ICCC 2016, and the WPMC 2016.

Ji Bian received the B.Sc. degree in electronic information science and technology from Shandong Normal University, Jinan, China, in 2010 and the M.Sc. degree in signal and information processing from Nanjing University of Posts and Telecommunications, Nanjing, China, in 2013.

He is currently pursuing the Ph.D. degree at the School of Information Science and Engineering, Shandong University, Qingdao, China. His current research interests include channel measurements, wireless propagation channel characterization, and 5G channel modeling.
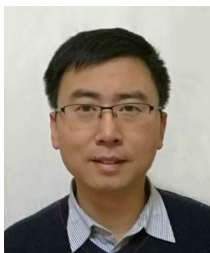
Jian Sun (M'08) received the BSc in Applied Electronic Technology, MEng in Measuring and Testing Technologies and Instruments, and PhD degrees in Communication and Information Systems, all from Zhejiang University, Hangzhou, China, in 1996, 1999 and 2005, respectively.

Since July 2005, he has been a Lecturer in the School of Information Science and Engineering, Shandong University, China. In 2011, he was a visiting scholar at Heriot-Watt University, UK, supported by UK-China Science Bridges: R&D on (B)4G Wireless Mobile Communications (UC4G) project. His current research interests are in the areas of signal processing for wireless communications, channel sounding and modeling, propagation measurement and parameter extraction, MIMO and multicarrier transmission systems design and implementation.

Wensheng Zhang received the M.E. degree in electrical engineering from Shandong University, China, in 2005, and the Ph.D. degree in electrical engineering from Keio University, Japan, in 2011. In 2011, he joined the School of Information Science and Engineering, Shandong University, where he is currently an Associate Professor. His research interests lie in cognitive radio networks, random matrix theory, and visible light communications.

Minggao Zhang received the BSc degree in mathematics from Wuhan University, China, in 1962.

He is currently a Distinguished Professor with the School of Information Science and Engineering, Shandong University, director of Academic Committee of China Rainbow Project Collaborative Innovation Center, director of Academic Committee of Shandong Provincial Key Lab of Wireless Communication Technologies, and a senior engineer of No. 22 Research Institute of China Electronics Technology Corporation (CETC). He has been an academician of Chinese Academy of Engineering since 1999 and is currently a Fellow of China Institute of Communications (CIC). He was a group leader of the Radio Transmission Research Group of ITU-R.

Minggao Zhang has been engaged in the research of radio propagation for decades. Many of his proposals have been adopted by international standardization organizations, including CCIR P.617-1, ITU-R P.680-3, ITU-R P.531-5, ITU-R P.529-2, and ITU-R P.676-3. In addition, he has received seven national and ministerial-level Science and Technology Progress Awards in China.